JOINT EUROPEAN TORUS JET

JET–P(87)11

A. Tanga, K. Behringer, A. Costley, M. Brusati, B. Denne, A. Edwards, A. Gibson,
R.D. Gill, N. Gottardi, R. Granetz, P.J. Harbour, H. Jaeckel , M. Keilhacker,
E. Lazzaro, M. Malacarne, P. Morgan, P. Noll, J. O'Rourke, P. Stott,
D. Summers, J. Tagle and P.R. Thomas

Magnetic Separatrix Experiments in JET

Magnetic Separatrix Experiments in JET

A. Tanga, K. Behringer, A. Costley, M. Brusati, B. Denne, A. Edwards, A. Gibson, R.D. Gill, N. Gottardi, R. Granetz, P.J. Harbour, H. Jaeckel , M. Keilhacker, E. Lazzaro, M. Malacarne, P. Morgan, P. Noll, J. O'Rourke, P. Stott, D. Summers, J. Tagle and P.R. Thomas

JET-Joint Undertaking, Culham Science Centre, OX14 3DB, Abingdon, UK

Preprint of Paper to be submitted for publication in
Nuclear Fusion

ABSTRACT.

Magnetic separatrix configurations have been produced in JET for plasma currents of up to 3MA. Experimental results obtained with these configurations show that some features can be achieved that are common to divertor tokamaks. In Ohmic discharges, high recycling regimes can be produced. In neutral beam heated discharges, substantial improvement of the energy confinement time is achieved together with the characteristic signatures of an H-mode. These characteristics include improved particle confinement, flatter density profile, and an increase in electron temperature especially at the edge, leading to a characteristic pedestal feature. At higher neutral beam power, higher plasma densities are reached, with deterioration of beam penetration and strong radiation losses in the outer region of the plasma. The global energy confinement time in the H-mode is observed to degrade with additional power. However, results of radial power balance analysis suggest that in the central region, where the radiation is not important, the degradation of confinement is small.

1. Introduction

JET (Joint European Torus) was conceived as a tokamak with the ability to approach plasma conditions appropriate to a thermonuclear reactor. The achievement of this goal depends on the optimisation of all the fusion parameters: plasma density, temperature and energy confinement time.

Overcoming, or at least reducing, the deterioration of confinement with intense additional heating is crucial to the achievement of these objectives. A substantial improvement in the transport properties of the plasma has been an important feature of tokamaks with a poloidal divertor in the H-mode.

In these experiments the divertor configuration, whose important feature is the presence of a magnetic separatrix, was supplemented by either a divertor chamber as in ASDEX[1] and PDX[2], or by a large volume as in D-III[3]. JET can produce a magnetic separatrix configuration but without a divertor or large ballast vacuum region. The distance between the X-point and the target plates is at most only a few centimeters. However the experimental results reported here show that the plasma behaviour is changed in a similar way to divertor tokamaks. High recycling regime has been observed in ohmic high density discharges, and, with neutral beam heating power larger than 5MW, a regime of enhanced energy and particle confinement has been produced. Typical features of this regime are similar to those observed in ASDEX and PDX in the H-mode, such as the sudden reduction of recycling, as a consequence of improved particle confinement, build up of a temperature pedestal at the plasma edge and a

global reduction of thermal transport. The relative quiescence of the JET H-mode makes it much more akin to the Edge Localised Modes (ELM) free phase in ASDEX [4] and to the H-mode found in DIII-D [5] than to the behaviour of the normal H-mode observed in ASDEX [1] and in PDX [2].

The first section of this paper is devoted to the analysis of the magnetic separatrix configuration in JET. In section 3 and 4 global characteristics and the confinement properties of the H-mode are discussed. The presence of a magnetic separatrix changes the boundary conditions of the discharge and a section is devoted to these phenomena. The behaviour of impurities and particle transport is then analysed and the final section is devoted to a preliminary analysis of energy transport and to the problem of confinement degradation with additional heating.

2. Plasma Equilibrium

2.1 Plasma Shape

JET is a tokamak designed to produce plasmas with elongated and D-shaped cross-sections. This is achieved by feedback control of currents in the shaping coils P2 and P3, shown in Fig 1, the details of the feedback system have been described elsewhere [6].

The P2 and P3 coils produce a mainly quadrupole field which controls the plasma elongation. A net hexapole field, which controls the plasma triangularity, can also be produced by causing oppositely directed currents to flow in these two pairs of coils. In addition to the field produced by the shaping coils, the effects of small aspect ratio and the

attraction of the iron core causes the plasma to have a natural elongation of about 1.4 in the presence of a purely vertical field (such as that created by the equilibrium coil P4). A second source of hexapole field is the main transformer coil P1, due to the leakage field produced by the iron collars at the top and bottom of the central column. For a large current in the P1 coil (-22MA), the flux in the equatorial plane is:

$$\psi\,(R,\ Z=0) = -17 - 0.071\left[\frac{R-R_o}{a_\nu}\right]^2 - 6.8\left[\frac{R-R_o}{a_\nu}\right]^3 - 3.9\left[\frac{R-R_o}{a_\nu}\right]^4 . \qquad (1)$$

Where R(m) is the major radius coordinate, $R_o = 2.96$m, ψ is in Weber and a_ν(m) is the mean minor radius of the vessel. The hexapole moment is proportional to the coefficient of $\left(\frac{R-R_o}{a_\nu}\right)^3$ and the octupole moment is proportional to that of $\left(\frac{R-R_o}{a_\nu}\right)^4$. The source of the hexapolar field of the iron core can be identified as due to the particular slope of the unsaturated iron collars. From a calculation, made using a Schwarz-Christoffel transformation of the polygonal boundary of the iron core [7], the combined hexapolar moment contribution of shaping coils and the iron leakage field, proportional to the primary current I , can be evaluated as:

$$M_H = \frac{\mu_o I_H}{\pi R_c^3} - \frac{\mu_o I_1}{\pi R_c^3}\alpha \quad . \qquad (2)$$

Where α is typically 10^{-2}, I_1 is the current in the primary circuit, I_H is the shaping coils current, R_c is the distance between the coil and the magnetic axis of the plasma. The first term on the r.h.s. represents the effect of the shaping coils, the second term represents the contribution of the primary current leakage field of the coil P1, which, in its negative swing phase, produces a shaping effect in addition to that of the P2 and P3 coils.

2.2 The Formation of a Magnetic Separatrix

By increasing the multipolar fields at a given value of plasma current, it is possible to produce a D shaped plasma whose two stagnation points are pulled inside the vessel, corresponding to a double-null configuration. By unbalancing the up-down shaping currents, a configuration in which only one of the two stagnation points is inside the vessel can also be achieved, corresponding to a single null configuration.

Two typical flux plots for single- and double-null configurations are shown in Fig 2. The distance between the X-points and the protection plates is a roughly linear function of the shaping current, as is shown in Fig 3. Magnetic separatrix configuration experiments have been performed with a current ratio of -40/24 for P2 and P3 coils for double-null configuration, producing an elongation of ~ 1.8; and a ratio of -20/16, (upper coils P2 and P3 only), for single-null configuration, which has a lower elongation of 1.65. This lower value is due to the lower contribution of the quadrupole field proportional to the difference in currents between P2 and P3 compared to the hexapole field. The vertical

position was adjusted by varying the radial field coil current on a time scale of about one third of a second.

2.3 Stabilization of Vertical Plasma Position

The vertical plasma position is unstable in JET for plasma elongation larger than 1.2. The relation between the growth rate of the vertical instability and the plasma parameters has been described elsewhere [6]. In general terms, the destabilising force on the plasma, displaced by δZ_p from the original position, can be described by $F = 2A_{pp}'' I_p^2 \delta Z_p$; where I_p is the plasma current and the coefficient

$$A_{pp}'' = -\frac{\pi R}{I_p}\left\{\left[\left(\frac{\overline{\delta B}_R}{\delta Z}\right)\right]_{equil} + \left[\left(\frac{\overline{\delta B}_R}{\delta Z}\right)\right]_{iron}\right\} . \qquad (3)$$

Where $\left(\frac{\overline{\delta B}_R}{\delta Z}\right)_{equil}$ is the gradient of the quadrupole component of the equilibrium field, $\left[\left(\frac{\overline{\delta B}_R}{\delta Z_p}\right)\right]_{iron}$ δZ_p is the radial field change caused by the iron circuit when the plasma current is displaced by δZ_p. The radial field gradients and variations are averaged over the plasma cross-section. By using the Shafranov equation the parametric dependence of A_{pp}'' can be written:

$$A_{pp}'' \simeq \frac{\mu_o R}{a^2+b^2}\left[\frac{b-a}{b+a}\right] P_q - \frac{3\mu_o}{16R}\left[\left(\ell n \frac{8R}{\bar{r}_p} - \frac{17}{12}\right)\right] . P_T + \frac{\mu_o R}{2\bar{r}_m^2} \qquad . \qquad (4)$$

Here $\bar{r}_m$ is the average effective distance of the magnetic circuit from the

plasma centre, $\bar{r}_p$ is the average plasma minor radius, a is the minor horizontal plasma radius, b is the minor vertical plasma radius, the coefficients P_q and P_T take into account plasma current effects and are equal to 1 for a flat current profile. The first term describes the effect of non-circularity, the second term represents a toroidal stabilizing effect, and the last term describes the effect of the iron. The agreement between the values derived from formula 4 and those calculated by using a full equilibrium code is fairly good, and is within 20% for limiter, double-null and single-null configurations. Since the main coefficient A''_{pp} in the formula for the vertical destablising force depends essentially on plasma elongation, plasma current profile and geometrical factors, it can be concluded that magnetic separatrix configurations are no more vertically unstable than symmetric limiter configurations with the same size, elongation and plasma current profile.

The stabilisation of vertical plasma position during a disruption with fast current quench is, however, more difficult in single null configurations. In limiter discharges the vertical position is kept centred on the midplane. In the single null configuration, instead, the position of the effective current centre is usually displaced from the midplane by some value Z_o. Rapid change of the plasma current then induces voltages proportional to Z_o multiplied by the time derivative of the plasma current both in the radial flux measurement and in the radial field coil. Therefore the stabilising circuit receives a perturbation right from the beginning of the disruption. Consequently during the disruption the voltage limits of the radial field amplifier can be reached, so that the stabilisation is disabled and the disruption is

accompanied by an escalating vertical plasma displacement. The actual displacement is expected to depend on the ratio of instability growth time to the current quench time.

Moreover, even in single-null configuration discharges arranged to have $Z_o \simeq 0$, because the decay time phase of the plasma current is much faster than the decay time of the shaping coil current. This produces large values of the quadrupole and hexapole field, compared to plasma current, which exceed the stabilization limit. In all cases the vertical plasma movement is directed towards the X-point.

3. Effects of Magnetic Separatrix in Ohmic Discharges

The magnetic separatrix configuration is usually produced during the current flat top of well established limiter discharges. The current in the shaping coils is raised in about 1s. During this time the plasma elongation is increased until a magnetic separatrix configuration is produced. This configuration can then be maintained for several seconds. In order to achieve a magnetic separatrix configuration at the highest plasma currents, use must be made of the combined effects of the primary coil leakage fields and of the shaping coils. In this case, the magnetic separatrix configuration is produced for several seconds at the end of a plasma current flat-top when the current in the primary coil is large. The magnetic configuration is deduced from the equilibrium identification code IDENT B [8] suitably modified for accurate determination of field null location [9]. The precision of the magnetically determined position of the X-point is 3÷5cm and within this distance it coincides with the position deduced from TV camera observations. Both the radial and

vertical position of the X-point are held constant within a few centimetres by the position control system. The X-point location is only weakly sensitive to changes of internal plasma parameters produced, for instance, by additional heating. The time evolution of the main signals for an X-point discharge is shown in Fig 4. During the magnetic separatrix configuration the deuterium recycling (monitored by D_α light) shifts from the outer limiters to a small area around the X-point. Simultaneously, the value of Z_{eff} drops. The average plasma density tends to decrease, a deuterium gas puff of 50÷100mbar/ls is needed for the first couple of seconds to sustain the plasma density at a constant value. When the separation between the plasma and the outer limiter is larger than 7cm, the limiter recycling virtually disappears. Even in the double-null configuration, TV observations in the near infra-red show the formation of a bright region, of approximately 20cm across, coinciding with only one of the X-points. The X-point which emits large radiation is the same even if the plasma is moved vertically, by as much as 20cm, causing the nominal double null configuration to become a single null one, suggesting that this is not connected with slight up-down asymmetries of the poloidal field. The radiating X-point is the one in the ion drift direction although this drift direction was not changed in the experiments. Consequently the asymmetry may be due to neoclassical ion effects such as those observed in ASDEX [10], where it was found that the power threshold for the H mode was lower when the ion drift direction was toward the X-point. Accordingly in the single-null configuration in JET the X-point was chosen to be in the ion drift direction.

In ohmic magnetic separatrix discharges, the value of the global energy confinement time is somewhat larger than that of the corresponding limiter

discharges. In particular, for comparable plasma density and current, plasma temperatures are similar but the loop voltage is somewhat lower than in limiter discharges, so that the confinement times are longer. In Fig 5 the values of global confinement time for the double-null configuration are plotted together with that of limiter discharges with same current (2MA) and toroidal field. The horizontal axis is the scaling factor $n_e\ q_{cyl} R^2 a$, which roughly represents the JET ohmic confinement [11]. The difference in confinement between the X-point and the limiter discharges is beyond experimental error. However, one cannot at present exclude the possible effects of different elongation and Z_{eff} in the scaling.

The presence of a high density region, which is a key feature of divertor plasma experiments, has been clearly detected in the JET ohmic discharges. During the magnetic separatrix configuration, the number of fringes measured by the interferometer channel intercepting the X-point shows an increase, while the average plasma density is approximately constant. This can be used to estimate the local X-point density. Assuming that the radius of the high density plasma region is of the same order as the highly radiating region seen by the bolometer and TV camera (~20cm across), this leads to densities of the order of ~ 1 - $2 \times 10^{20} m^{-3}$. In high density discharges, the small area around the X-point is capable of radiating up to 50% of the input power. The power radiated from this region scales roughly with the square of plasma density and it is similar in double-null and in single-null configurations.

4. Neutral Beam Heating of Single-Null Discharges

4.1 Time Evolution

Heating experiments have been performed in single-null discharges with deuterium co-injection at energies up to 80keV per deuteron, in deuterium plasmas. The pulse length was limited to <4s to avoid thermal overloading of the graphite target tiles. Experiments were carried out at plasma currents of 1, 2 and 3MA and toroidal fields between 2.0T and 3.4T. The relative direction of toroidal field and plasma current was chosen to have the ion drift directed toward the X-point, which was in the upper part of the vessel. Typically, the time evolution of such a discharge shows three characteristic phases which are shown in Fig 6 for a 2.0MA discharge with ~7MW of total input power. In the first 0.5 s of neutral beam heating, the plasma density increases slowly, the total stored energy increases up to a value somewhat larger than that expected for a limiter discharge with similar parameters. This phase has been called the L-phase. In this phase the plasma does not show characteristic features of an H-mode: the D_α signal monitoring the particle flux to the wall is high, with a low value of the particle confinement time. This phase, described later, is also characterised by intense edge MHD activity and by rapid losses of particles, corresponding with edge relaxations, detected by the D_α array. The value of stored energy is somewhat larger than that of corresponding limiter discharges, indicated by a dotted line in Fig. 6

After 0.5 s, and often at a sawtooth crash, a transition occurs: the density starts to increase at a much higher rate and so does the total stored energy. The plasma density increases at a faster rate than the

beam fuelling. The D_α signal drops at both the plasma boundary and at the X-point, the edge temperature profile steepens and stays constant, (as shown at 10cm within the separatrix in Fig 6). The global energy confinement time increases to a higher value. This phase has been called the H-phase because it shows characteristic behaviour of the H-mode discharges found in other tokamaks [1,2,5] such as: a) the existence of a power threshold; b) a preceding L-phase; c) simultaneous improvement in energy and particle confinement; d) a drop in recycling signals and e) development of high edge electron temperatures. In JET the H-mode could be obtained only for power levels exceeding 5MW at a toroidal field of 2.1T. This level is practically independent of plasma current. The threshold power was 9MW for toroidal field of 2.8T and, with the power presently available, it has not been possible to produce an H-phase at toroidal fields of 3.4T. Magnetic separatrix discharges which fail to achieve an H-mode show L-phase behaviour for the entire duration of the beam pulse. At the transition to H-phase, MHD fluctuations and the edge relaxations stop (as described in Sect. 5). During the H-phase, the increase in density causes the beam particles and power to be deposited more and more in the outer regions of the plasma column. The impurity concentration, which increases slightly, causes build up of the radiated power mostly from the outer half plasma radius reducing the power conducted to the separatrix. When this power flow drops below threshold, the H-mode collapses, reverting back into an L-mode. The H to L transition is characterised by the release of plasma energy gained during the H-phase. This energy is mainly conducted to the separatrix dump plates in times of ~ 50ms causing large excursions of the surface temperature of the dump tiles. In this phase the plasma density falls rapidly and the radiated power is reduced. With sufficient neutral beam

power, subsequent further L-H transitions can take place. As described in sect. 5, during the H-mode there are no indications of the high recycling regime, which is observed in ohmic plasmas (c.f. section 3).

4.2 Global Energy Confinement

The main results achieved in the H-mode are summarised in Figs 7 and 8, which show the total stored energy and the global energy confinement time as a function of the total input power. The confinement data are shown for plasma currents of 1, 2 and 3MA for limiter, L- and H-phases. Fig 7 shows the total stored energy versus total input power for the same discharges as in Fig 8 with the addition of the values of the magnetic separatrix discharges in the L-mode. The latter were chosen among discharges with values of toroidal field of 3.0 to 3.4 Tesla for which, presumably, the threshold power for the transition to the H-mode is larger than that available. The energy confinement for the L-mode is between the limiter values and those of the H-mode.

In Fig 8, the H-mode points have energy confinement times more than a factor of two larger than limiter discharges at the same current. It is also evident that in the H-mode the energy confinement time scaling is approximately proportional to the plasma current.

The values for the H-mode points have been selected towards the end of the H-phase when the derivative of the plasma energy content is small compared to the total input power. However, the maximum value to which the plasma density climbs during the H-mode is a function of the input power itself and this is shown in Fig 9. The dependence can be approximated by a slope $(P-P_o)^{0.5}$. Input power and plasma density are then coupled and it is

difficult to extract a parametric dependence of the confinement time on plasma density. These densities correspond to values of the Murakami parameter 20% higher than those otherwise possible in ohmic or neutral beam heated limiter discharges.

In the H-mode the values of energy confinement time decrease with increasing power; the problem of confinement degradation in the H-mode is analysed in the final section of this paper.

4.3 Electron Temperature Profiles

A typical sequence of electron temperature profiles from electron cyclotron emission analysis is shown in Fig 10, where constant neutral beam power is applied and the discharge goes from the L to the H-phase. During the initial L-phase the temperature increases, with a roughly constant profile shape. The transition to the H-phase is characterised by an abrupt increase in the edge temperature, similar to the "pedestal" observed in ASDEX [1] and PDX [2]. The outermost point which can be measured by the second harmonic of electron cyclotron emission is at R = 4.0m so that the electron temperature at the separatrix radius (at R = 4.1 m), cannot be determined. During the H-phase, the plasma density increases continuously and the average electron temperature increases slightly, at the highest plasma densities the average electron temperature may fall slightly before the end of the H-phase.

The broadening of the electron temperature profile can be deduced also from the X-ray tomographic reconstruction shown in Fig 11. The emission in the edge region increases substantially and during the H-mode the volume

of plasma emitting X-rays increases to nearly the whole plasma cross-section. The change in profile shape is also clearly seen in the plot of the second moment (a measure of the profile width) of the X-ray data from the vertical camera shown in Fig 12. The second moment increases by 30-40% during an L to H transition and this change is a clear indicator of the existence of the H-mode. The observation of X-ray emission from close to the plasma boundary indicates that the electron temperatures in this region are roughly double those observed in the L-phase. After the H-mode transition, both the amplitude and inversion radius of sawteeth decrease, and the period also decreases.

4.4 Electron Density Profiles

The electron density profiles of both ohmically heated and L-mode neutral beam heated X-point discharges are similar to those obtained in limiter and inner-wall discharges, having a profile ($n_e = n_{eo} (1-\rho^2)^{0.5}$). The transition from L-mode to H-mode, is marked by a pronounced broadening of the density profile. A typical sequence of density profiles is shown in Fig 13. Spatially resolved measurements of the D_α light indicate that the total electron source decreases during the L-mode to H-mode transition. Thus the behaviour of the density profile must be attributed to a net decrease in the outward flux of particles during the transition to the H-mode.

Changes in particle transport can be analysed using a simple model in which the electron flux Γ_e can be described with an expression of the form [12]:

$$\Gamma_e = -D_p \nabla n_e - \Gamma_p \quad . \qquad (5)$$

Here D_p is the diffusion coefficient and Γ_p is an inward particle flux. For typical values of the diffusion coefficient, (~0.6m²/s), the flattening of the density profiles during the H-mode implies that the ratio Γ_p/D_p is doubled at r/a ~ 0.75. Toward the end of the H phase the density profiles are very flat ($n_e = n_{eo}\,(1-\rho^2)^{0.25}$). At the H to L transitions the density falls and the density profile rapidly reverts back to the more peaked shape characteristic of the L-mode, as shown in Fig 14.

4.5 Current Density Profiles

Indications of current density profile changes during the H-mode can be derived from the time evolution of internal inductance.
The values, calculated with the magnetic code [8], are shown together with the poloidal beta in Fig 15. The value of ℓ_i drops during the H-mode indicating a flattening of current profile distribution. A full reconstruction of the MHD equilibrium, by fitting the magnetic data shows that a good fit can be obtained only with current profiles which, instead of being typically bell shaped, have shoulders at the plasma edge. This is in agreement with the increase of edge temperature reported above.

5. Plasma Edge and Scrape-off

5.1 Edge plasma fluctuations

The H-mode has been associated with characteristic behaviour of the magnetic fluctuations at the plasma edge in D-III [13] and to Edge Localised Modes in ASDEX [4]. In JET the L-phase of the discharge is characterised by edge fluctuations extending along the full poloidal circumference. These fluctuation disappear at the L to H transition. The physical nature of the edge fluctuation described here is probably different from the ELM's observed in ASDEX [4]. Whilst the ELM's observed in ASDEX occur after a quiescent phase and are triggered by the edge pressure gradient reaching a limit value, the fluctuations observed in JET are associated with L-mode, they preceed the H-phase and the plasma pressure has a low value. These are present for the whole duration of the beam pulse in discharges with insufficient power for the L to H transition. The JET L-phase fluctuations are clearly visible on the soft X-ray, fast MHD signals, reflectometer and D_α multichannel signals. The level of magnetic turbulence, (in the frequency band 5-60kHz), is enhanced by the presence of neutral beam heating; whenever an L to H transition occurs signals of the magnetic pick-up coils close to the single-null show a marked and sudden drop, as shown in Fig 16. This figure shows the good time correlation existing between the level of magnetic turbulence (at about 40kHz) and the H and L phases of the discharge.

The L-H transitions are always preceded by regular disruptive-like events at the plasma edge. The mode is seen in most X-ray channels as a disruptive-like instability with a sudden drop in X-ray intensity. A more detailed study of these fluctuations, using data taken at 200kHz, shows that in the outermost channel the change in intensity occurs very rapidly (80μs) whereas in other channels at smaller radii the change is much

slower (800μs). This indicates a mode occurring in the edge region with its effects becoming slower as it propagates inwards.

The traces of the pick up coils, which detect the magnetic part of the fluctuations, during the L-phase, feature regular spikes which are correlated with each edge disruption observed by the X-ray signal. This is shown in detail in Fig 17(a),(b). Sawtooth crashes decrease the repetition frequency of these edge modes and generally the final transition coincides with one of these crashes as shown in Figs 18(a) and (b). The second example, in Fig 18c-d, shows the magnetic activity during a typical H-L transition. This transition is accompanied by a burst of broad band magnetic activity which lasts for times comparable to the relaxation of the density and temperature profiles.

5.2 Plasma Scrape-off Measurements

Scrape off parameters are measured by a Langmuir probe. The vertically moveable probe can scan a region on the top of the machine at a major radius R=3.2m. In discharges with additional heating a vertical scan can be performed up to a distance of 5 cm from the magnetic separatrix.

The temporal variation of the probe saturation current, i_{SAT}, is shown in Fig 19 with the D_α signal taken along a vertical chord. Beams were switched on at 9.5 seconds, the H-mode was achieved from 12 to 13.6 seconds. The scrape off electron density is approximately constant during the H-mode despite a three-fold increase in plasma density. This contrasts with limiter and L-mode discharges where the density, in the

scrape off, increases approximately with the square of the average electron density. There is a significant transient rise in i_{SAT} with the termination of the H-mode. This is associated with the rapid loss of confinement at the H to L transition.

5.3 Particle Balance and Recycling Coefficient

A common feature of H-mode observed in JET as well as in ASDEX [1], PDX [2], DIII-D [5] is the rapid increase in plasma density which takes place after its onset. In the H-mode the particle fluxes from the plasma are reduced as seen by the drop of D_α signals. Using the data from a poloidal array of D_α detectors the global particle balance equation has been solved [14]. The resulting time evolution for the global particle confinement time and global recycling coefficient is shown in Fig 20. In the ohmic discharges with magnetic separatrix the values of particle confinement time are lower than in the limiter configuration and during the L-phase there is a degradation of τ_p similar to that observed in limiter discharges. At the onset of H-mode the value of τ_p doubles stepwise and stays roughly constant throughout the H-phase. Since the rate of increase of plasma density is up to a factor two larger than the fuelling rate, the values of the recycling coefficient are larger than one, this effect is further enhanced by the increase of τ_p.

A comparative plot of τ_p for limiter, L and H mode discharges is shown in Fig. 21 versus average plasma density. The limiter discharges are characterised by values of particle confinement time that decrease with increasing density, essentially as a result of higher edge plasma densities. In contrast, with magnetic seperatrix, two regions exist: at

low densities, in the L mode, the value of τ_p is lower than in the limiter discharges while in the H mode it is higher. In the H-mode the particle fluxes from the plama, as measured by D_α array, are small. This is in agreement with small values of saturation current measured by the Langmuir probe. These observations, the indication of high edge temperatures (c.f. sect. 4.3) and the comparative low level of radiation from the X-point region (c.f. Fig. 6 and sect. 6.2) indicate that there is no high recycling region in the H-mode.

6. Behaviour of Impurities and Radiation Losses

Spectroscopic diagnostics (XUV, VUV, Visible and Charge Exchange Recombination Spectroscopy (CXRS) have been used for studying impurity behaviour in JET plasmas during magnetic separatrix operation. The main impurities in JET plasmas are carbon (from carbon limiters and protection plates) and oxygen. Metals (nickel and chromium from Inconel walls and antenna screens) generally contribute little to Z_{eff} and radiated power. Typical impurity concentrations (in % of the electron density, n_e) are [15]: 2-4% C, $\sim$ 1% O, and 0.02%, or less, metals. During the period in which most of the X-point operation was carried out, the oxygen concentration in the plasma was, however, somewhat higher ($\sim$ 2%) due to occasional vacuum leaks.

6.1 Ohmic Discharges

Compared to similar limiter discharges Z_{eff} was somewhat lower in X-point

plasmas (Fig 22 - filled circles), essentially due to a reduced carbon concentration (1-2% C during X-point). The reduction implies that less carbon was produced at the X-point graphite target plates than at the limiters. Metal concentrations were reduced too, although the dump plates were most likely covered by wall material. During previous operation with Inconel dump plates no increase was observed in metal concentrations in the plasma when changing from carbon inner-wall to X-point operation. These observations indicate a low plasma temperatue ($\tilde{<}$ 20eV) in front of the plates characteristic of the high recycling zone described above, resulting in a low sputtering yield. A change in the screening property of the boundary plasma is a less likely explanation, results on ASDEX [16] showing that the screening is comparable in divertor and limiter plasmas. The oxygen concentration, oxygen most likely originating from the vessel walls, was 1-2% n_e, similar to limiter palsmas for the same plasma conditions.

6.2 Discharges with Additional Heating

With Neutral-Beam Injection (NBI) both carbon and metal concetrations were higher than in the ohmic case, which is consistent with an observed increase in the edge electron temperature, although the metals might also have originated from CX sputtering. The C/O ratio increased during NBI, in contrast to what was observed in limiter plasmas, where oxygen was the dominating impurity during NBI at high $\bar{n}_e$. As shown in Fig 22 somewhat higher Z_{eff} values were found in X-point plasmas with additional heating - the general falling trend with increasing n_e, observed in ohmic cases,

being maintained. During Ion Cyclotron Resonance Heating (ICRH) and combined heating, increased levels of screen material (Ni and Cr) were found in the plasma as in the limiter cases [17].

During the H-mode, Z_{eff} did not decrease as normal at high $\bar{n}_e$ (see Fig 22), but remained similar to the lower-$\bar{n}_e$ values of 3-4. The high Z_{eff} values could be accounted for by the central concentrations of light impurities as measured by CXRS (Fig 23). The C/O ratio during H-mode was 1-2:1. An observed increase in metal density can be explained either by sputtering by CX neutrals or by the increased edge temperature. The metal concentration was relatively independent of $\bar{n}_e$ for H-mode plasmas which contrasts with the falling trend with increasing $\bar{n}_e$ seen in all other types of discharges (Fig 24). However, the metal concentration is still low: its contribution to Z_{eff} is ≤ 0.2 (Fig 25), and $\leq 10\%$ of P_{rad} is due to metals according to transport code calculations.

At the L-H transition the radiation from the peripheral ions (O IV- O VII lines) was essentially unchanged (or even decreased) after the L-H transition, whereas O VIII radiation, emitted from radial locations further in, increased roughly as $\bar{n}_e^2$. The behaviour of the lowly-ionised C and O is consistent with the observed change in edge parameters, and results in less total radiation per ion for these light impurities.

The bulk particle confinement increased by a factor ~3 in the L-H transition. The impurity confinement increased similarly. For carbon the improved confinement can be seen in Fig 23: the carbon concentration is

essentially constant, or increases somewhat in the H-mode, although the carbon influx (represented by the C III-line brightness) drops just as the hydrogen flux, ϕ_H (carbon production yield $\phi_C/\phi_H \sim 5\%$).

There is no indication of impurity accumulation in the neoclassical sense. Analysis of several metal ionisation stages as well as the soft X-ray emission profiles and bolometer show that the metal density profile is not peaked in the centre. The values of nickel concentration derived from Ni XXV, XXVI, (VUV spectrometer) and Ni XXVII (X-ray crystal spectrometer) line intensities agree to within a factor ~2, which is within the error bars. The absence of impurity accumulation might possibly be explained by the presence of sawteeth in the H-mode discharges.

The time evolution of radiation losses in an H-mode discharge is shown in the bottom traces of Fig 6. During the first L-phase the power radiated from the main plasma (P^{rad}_{bulk}) is of the order of 20% of the total input power. During the H-mode, the power radiated from the main plasma increases while the power radiated from the small region around the X-point is roughly constant (see Fig 6). When only neutral beam heating is applied the increase of the radiated power from the main plasma scales with the square of plasma density as is shown in Fig 25: the ratio of radiated power to square of the average plasma density is approximately constant during the H-phase while the average plasma density increases three times. This is in agreement with the result that Z_{eff} and the concentration of the main impurities are approximately constant during the H-phase. The increase in bulk radiation during the H-phase takes place essentially in the outer region of the plasma as is shown by the sequence

of Abel inverted radiation profiles shown in Fig 26, although the radiating shell penetrates more deeply inside the plasma at higher densities. The total radiated power can be accounted for by the radiation of oxygen and carbon, although the radiation profile is dissimilar to the usual light impurity edge shells. Metals should contribute little ($\leq$10%) unless their concentration was substantially underestimated, which is unlikely since all VUV and X-ray diagnostics yield consistently low results. Model calculations based on the usual transport coefficients fail to explain the broad shells seen by the bolometer, although a change in ionisation balance due to the presence of beam neutrals leads to some inward shift and broadening of light impurity radiation. It must be assumed that impurity transport is modified in the following way: a high inward drift velocity at the plasma edge leads to a steepening of impurity ion profiles and higher particle confinement. This profile change is confirmed by a comparison of nickel radiation from the plasma edge (Ni XVII, XVIII) and from the plasma interior (Ni XXV, XXVI). In the plasma centre, impurity ion profiles are hollow, probably due to the non-stationary nature of the H-mode discharges. On the basis of these assumptions, the bolometer profiles can be explained by the radiation of light impurities, essentially oxygen. The same transport model may explain the meausred density profiles during the H-mode. The power flow to the magnetic separatrix can be calculated from global power balance. The density related increase in radiation reduces the power flow to the magnetic separatrix, at the moment of H to L transition, this is found to be between 3.5 and 4.0MW, independent of the value of the input power. This indicates that the end of the H phase is connected to a threshold value for the power flow to the magnetic separatrix.

7. Transport Phenomena in H-mode discharges

Transport features of H-mode discharges in JET have been investigated using the 1½D time-dependent interpretation code JICS [18]. As experimental information on the ion temperature profile is not available, a large uncertainty exists in the evaluation of the electron-ion coupling power term which accounts for a non-negligible fraction of the power balance for both populations. The ion energy content can be modelled from the experimental information of the ion temperature on axis, provided by the X-ray crystal spectrometer and charge exchange spectroscopy and taking into account as a mild integral constraint the total plasma stored energy as measured by the diamagnetic loop. However, the strong electron-ion coupling which exists at the high flat profile electron density profiles typical of JET H-modes, suggests that the overall dynamics of these discharges is best dealt with using a single fluid approach.

It is found that the L to H transition triggers a reduction of transport losses over the whole plasma cross-section; this reduction is established during a time of the order of the confinement time and is then maintained for the whole H-phase. This is well correlated with the build-up of a thermal barrier at the plasma edge similar to that found on ASDEX [19].

In Fig 27, the total plasma stored energy is shown as a function of radius at different times during the H-mode. Two distinct phases can be observed: during the first phase a gradual build-up of the plasma energy content takes place, which can be attributed to reduced global losses; in the second phase increased radiation losses deplete the stored energy. As a result the total energy confinement time is affected, while the

confinement time in the inner transport dominated layers remains unaltered (Fig 28). Sensitivity analysis of τ_E on the ion temperature profile (not available experimentally) was carried out by varying T_i within a range ($\pm$ 20% locally) compatible with the strong electron-ion coupling, which occurs at these high densities.

The related uncertainty is found to be ~25%, i.e. less than the difference in behaviour of τ_E at <a> and <a>/2 as shown in Fig 28. No appreciable confinement degradation appears with increasing input power respect to ohmic values (Fig 29).

8. Conclusions

These experiments have focused on the study of physics parameters affected by operation with a magnetic separatrix. The analysis of plasma equilibrium shows that a magnetic separatrix configuration can be created in JET by suitable selection of currents in the coils used for control of the plasma elongation and triangularity and by the leakage field of the primary circuit.

The vertical stability of this configuration is not appreciably different from that of a limiter discharge with similar elongation. However, with magnetic separatrix configuration, plasma disruptions always tend to have a vertical instability component. Features typical of a divertor tokamaks have been observed in JET such as the formation of a high recycling regime in ohmic high density discharges. With neutral beam heating in the single null configuration an improved confinement regime has been observed when the total input power exceeded a threshold value of 5MW. This regime

shows typical signatures previously observed in H-mode discharges in ASDEX, PDX and DIII-D. Characteristics such as an increase of particle confinement and a quench of plasma edge instabilities measured by magnetic pick-up coils, soft X-ray, reflectometry and D_α emission have been observed. An improvement in global energy confinement by a factor of two compared to limiter discharges has been measured. During the L-phase confinement is somewhat improved over that in the limiter configuration but lower than the best confinement achieved in the H-phase.
In common with ASDEX, PDX and DIII-D H-mode, the JET H-mode shows a large increase in plasma density, flatter density profile, and an increase in electron temperature especially at the edge, leading to a characteristic pedestal feature. The dominant impurities are carbon and oxygen, and metal impurity concentrations, larger compared to limiter discharges, contribute only a small amount to the value of Z_{eff}. These relatively higher impurity concentrations may be explained by longer confinement times and/or by increased sources due to higher edge temperatures. In the lifetime of the JET H-mode, lasting at most 2 seconds, the radiation profile is characteristically hollow indicating no significant accumulation of impurities in the centre of the discharges. It should be noted however that the duration of the H-mode is much shorter than the time the incoming impurities need to reach the centre of the plasma, if the transport is purely neoclassical.

In the latter part of an H-mode the input power is deposited, and also radiated, increasingly in the outer layers of the plasma, due to the increase in plasma density and the higher concentration of impurities, until the H-mode collapses. The H-modes reverts to an L-mode when the power flowing to the separatrix falls below a threshold value.

Global energy confinement times degrade with power, but this degradation can be largely ascribed to poor beam penetration and to high radiation losses. Power balance calculations performed over the inner half only of the plasma radius, where radiative losses are still negligible, give indications that the central confinement does not suffer appreciable deterioration with power.

ACKNOWLEDGEMENTS

This paper contains experimental results which have been achieved by the dedication and efforts of all the JET Team. Particularly involved in the experimental work have been members of the Magnet and Power Supply Division, First Wall Division, the Neutral Beam Heating Division, Radio Frequency Heating Division and the Experimental Divisions. The efforts of J Christiansen in producing "Fast" code analysis of the magnetic configuration and K. Thomsen for the data management are acknowledged. We are grateful to R. J. Bickerton, J. G. Cordey, M. L. Watkins and A. Gondhalekar for the fruitful discussions, and to G Fussmann for preliminary analysis of spectroscopic data. Thanks are also due to P. Lomas and F. C. Schüller, for conducting experimental sessions, and to B E Keen for editorial work on the paper.

REFERENCES

[1] Wagner, F., Becker, G., Behringer, K., Campbell, D., Eberhagen, A., et al in Proceedings of the Ninth International Conference on Plasma Physics and Controlled Nuclear Fusion Research. Baltimore 1-8 Septemer 1982. IAEA-Vienna 1983, page 43; and Wagner, F., Becker, G., Behringer, K., Campbell, D., Eberhagen, A., et al Phys. Rev. Lett 49 1408 (1982).

[2] Kaye, S.M., Bell, M.G., Bol, K., Boyd, D., Brau, K., et al in Proceedings of the Symposium on Energy Removal and Particle Control in Fusion Devices Princeton, N.J., USA, 26-29 July 1983. North-Holland Physics Publishing Co, Amsterdam 1984, page 115.

[3] Ohyabu, N., Burrell, K., H., De Boo, J., Ejima, S., Groebner, R., Overskei, D., et al Nucl. Fus. 25 49 (1985).

[4] Keilhacker, M., Fussmann, G., Von Gierke, G., Janeschitz, G., Kornherr, M., et al in Proceedings of the Tenth International Conference on Plasma Physics and Controlled Nuclear Fusion Research London 11-19 November 1984, Vol I, page 71 (IAEA-Vienna 1985).

[5] Luxon, J., Anderson, P., Baity, F., Baxi, C., Bramson, G., et al "Initial results from DIII-D Tokamak" presented at Eleventh International Conference on Plasma Physics and Controlled Nuclear Fusion Research. Kyoto, Japan, 13-20 November 1986. Paper IAEA-CN-47/A-III-3. To be published.

[6] Bertolini, E., Mondino, P.L., Noll, P., Fusion Technology 11 (1987) 71.

[7] Bewley, L. V., in "Two dimensional fields in Electrical Engineering" Dover Publ. N. York (USA) 1963.

[8] Brusati, M., Christiansen, J.P., Cordey, J.G., Jarret, K., Lazzaro, E., Ross, R., Comp. Phys. Rep. 7-8 (1984) 345.

[9] Tanga, A., Campbell, D.J., Denne, B.D., Gibson, A., Gottardi, N., et al in Proceedings of 12th European Conference on Controlled Fusion and Plasma Physics, Budapest 2-6 September 1985, Published by European Physical Society, (Budapest 1985), Vol I, page 19.

[10] Wagner, F., Bartiromo, R., Becker G., Bosh, H. S., Eberhagen, A. et al., Nucl. Fus. 25 1490 (1985)

[11] Bickerton, R. J., Alladio, F., Bartlett, D. V., Behringer, K., Behrish, R., et al. in Plasma Physics and Controlled Fusion, 28 (1986) 55.

[12] Coppi, B. and Sharky, N., in Physics of Plasma Close to Thermonuclear Conditions, Proceedings of the course held in Varenna, Italy 27 August - 8 September 1979. Commission of the European Communities, Brussels. Vol I, page 47; and Behringer, K., Engelhardt, W., Feneberg, W., Fussmann, G., Bull Amer. Phys. Soc., 25 (1980) 875.

[13] Ohyabu, N., Jahns, G. L., Stambaugh, R. D., Strait, E. J., Phys. Rev. Lett. 58 120 (1987).

[14] Tanga, A., Gowers, C.W., Hugenholtz, C.A., Morgan, P., Schüller, F.C., "Global Particle Balance and Recycling in First JET Discharges". JET Report: JET-P(84)09.

[15] Behringer, K., Boileau, A., Bombarda, F., Denne, B., Engelhardt, W., et al. "Impurity production mechanisms and behaviour during additional heating in JET" presented at Eleventh International Conference on Plasma Physics and Controlled Nuclear Fusion Research, Kyoto, Japan, 13-20 November 1986. Paper IAEA-CN-47/A-IV-1. To be published.

[16] Engelhardt, W., Becker, G., Behringer, K., Campbell, A., Eberhagen, A., et al. J of Nucl. Mater. 111&112 337 (1982).

[17] Behringer, K., Denne, B., Forrest, M. J., Hawkes, N. C., Kaye, A., et al, in Proc. of the 13th European Conference on Controlled Fusion and Plasma Heating, Schliersee, 14-18 April 1986. Published by European Physical Society, Vol 10C, Part I, p.176.

[18] Brusati, M. and Cordey, J. G., in Proceedings of 12th European Conference on Controlled Fusion and Plasma Physics, Budapest, 2-6 September 1985, Published by European Physical Society, (Budapest 1985), Vol I, p.34.

[19] Gruber, O., Jilge, W., Bernhardi, K., Eberhagen, A., Fussmann, G., et al in Proc. of 12th European Conference on Controlled Fusion and Plasma Physics. Budapest 2-6 September 85 Vol I, p.18 (Budapest 1985).

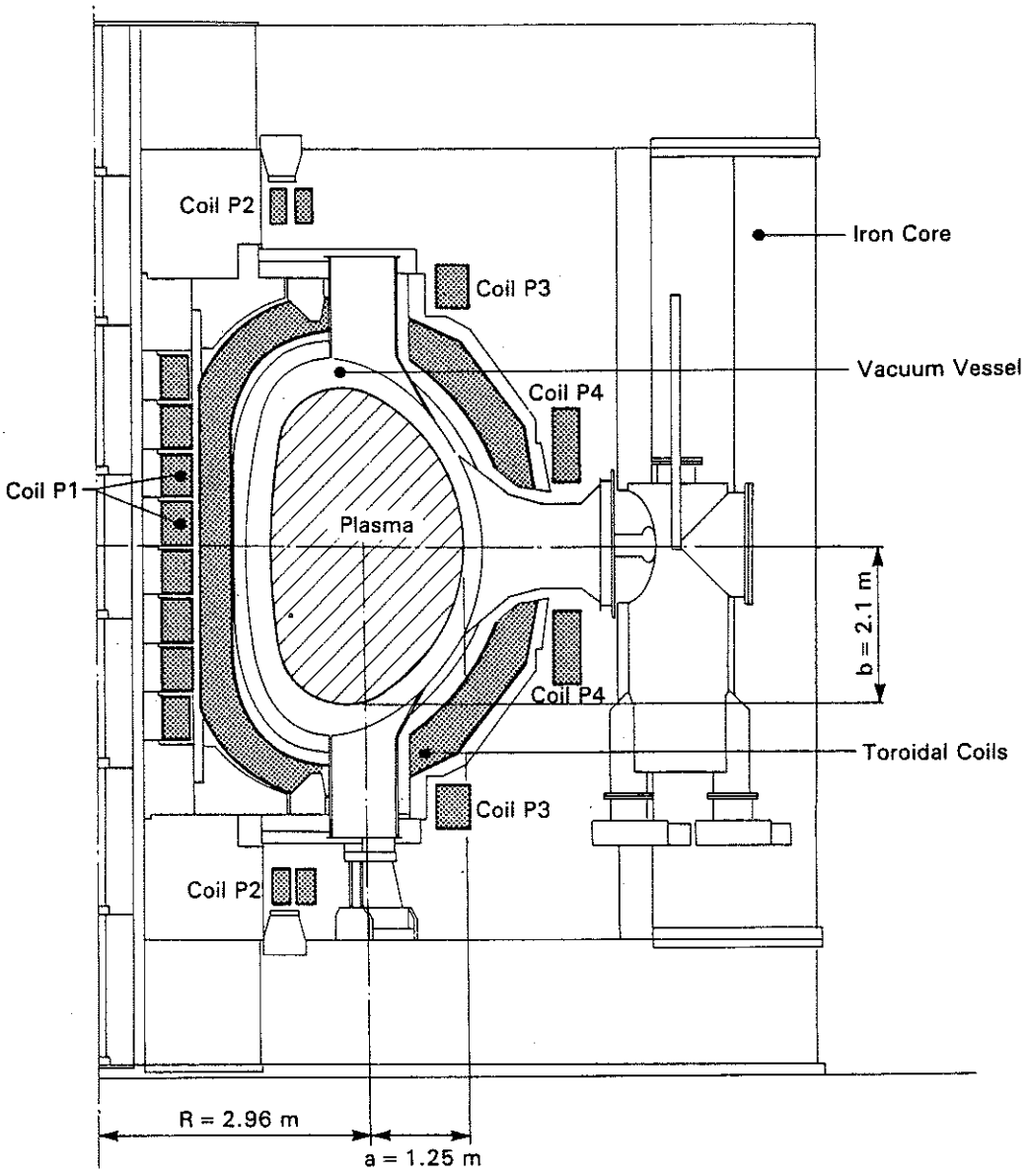

Fig 1 Cross-sectional view of JET showing the location of various coils.

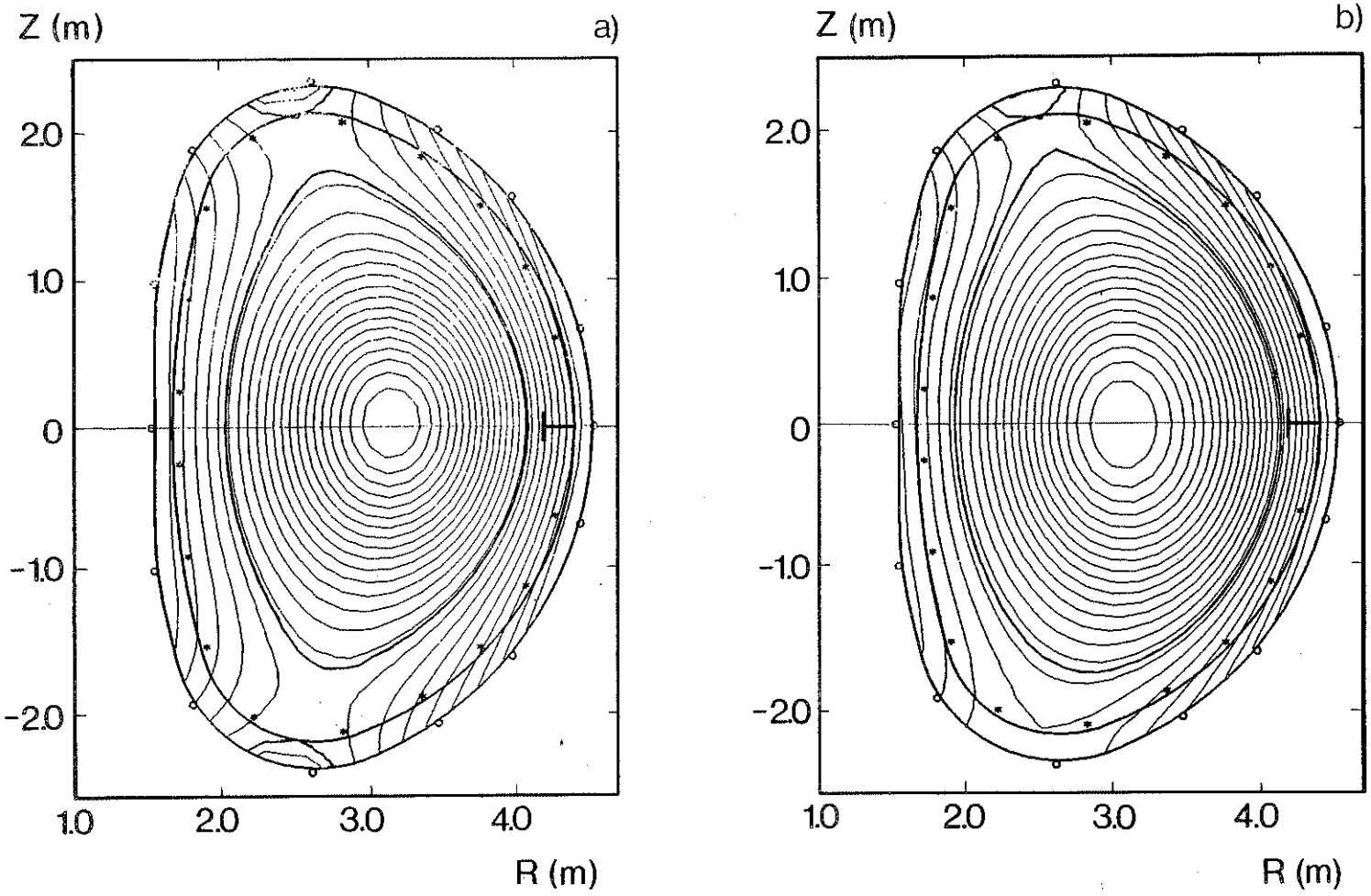

Fig 2 (a) Flux plot of a double null configuration. Plasma current = 2MA, toroidal field 2.8T, plasma electron average density = $3.10^{19}m^{-3}$, poloidal beta = 0.44, plasma elongation = 1.8.

(b) Flux plot of a single null configuration. Plasma current = 2.0MA, Toroidal field = 2.2T, plasma electron average density = $3.10^{19}m^{-3}$, poloidal beta = 0.6, (Pulse No 10237, t = 13.5s).

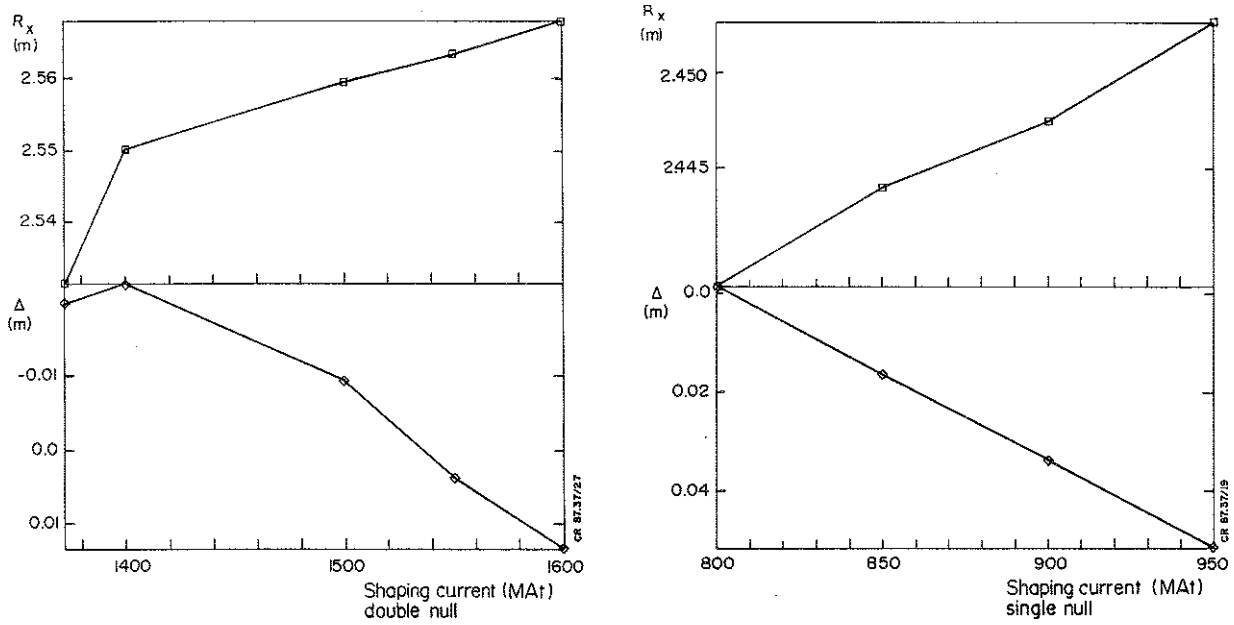

Fig 3 Calculated major radius of the X-point R_x, and Δ distance of the X-point from the target tiles versus the total shaping current in the coils P2 and P3 (with the turn ratio as in the text), at moderate primary current.

(a) Double-null configuration at plasma current of 2.0MA.

(b) Single-null configuration at plasma current of 2.0MA. The value of the major radius co-ordinate of the X-point is virtually independent of the shaping current. The sign of Δ is chosen to be positive for X-point within the vessel aperture.

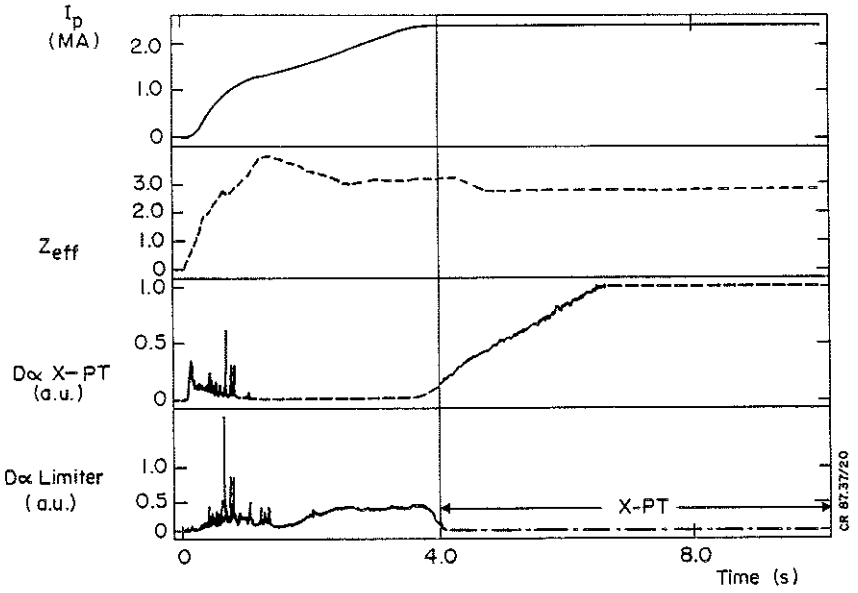

Fig 4 Time evolution of a typical ohmic discharge with magnetic separatrix. From the top, plasma current, ion effective charge measured by visible bremsstrahlung, intensity of D_α radiation from the X-point and from the limiter.

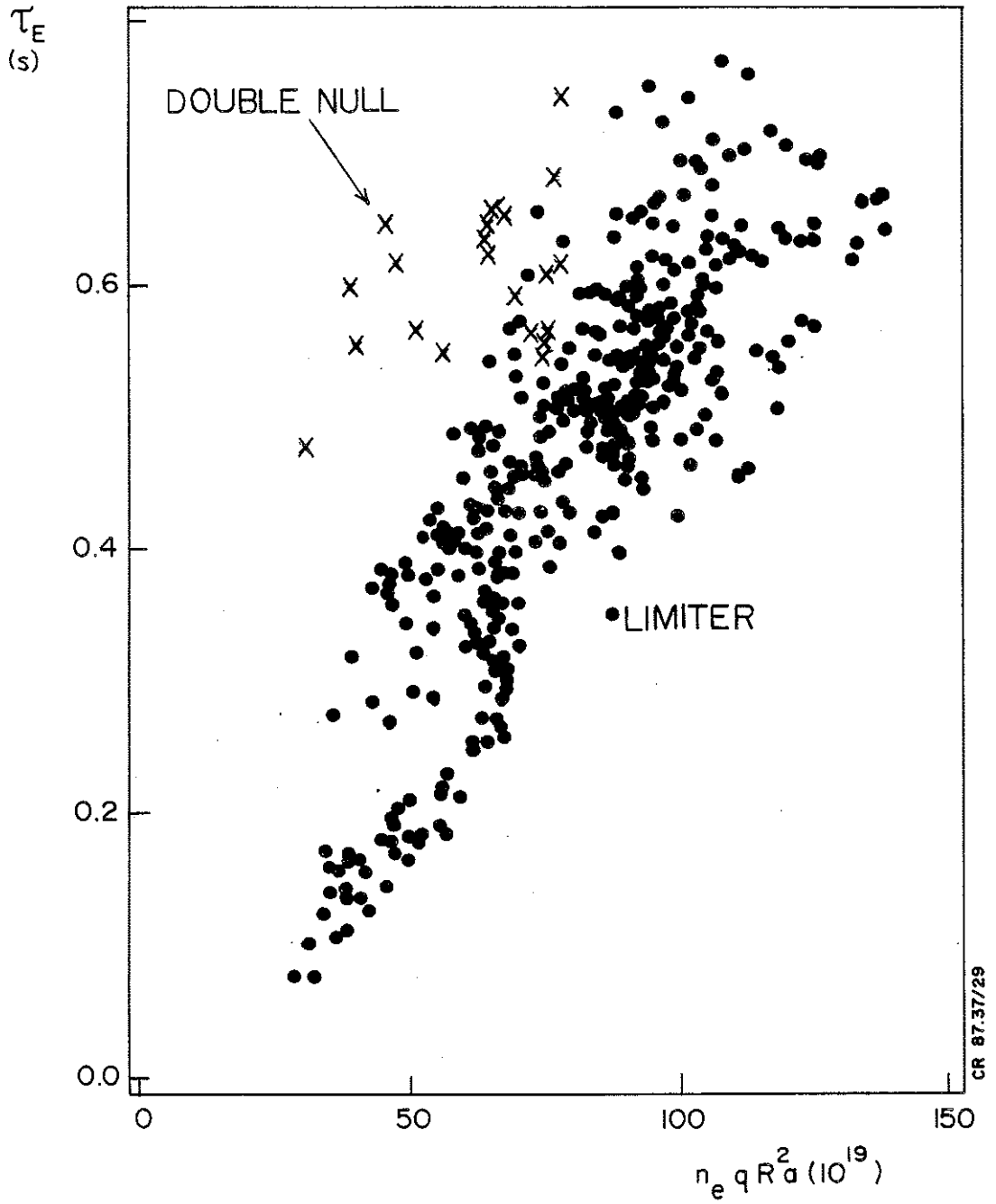

Fig 5 Energy confinement plot for magnetic separatrix and limiter ohmic discharges at plasma current of 2.0MA$_T$ versus neo-Alcator scaling. Note that the best fit of JET ohmic data scales as $\tau_E \alpha\ R^{1.7}\ a^{1.3}\ q\ n_e^{0.4}$.

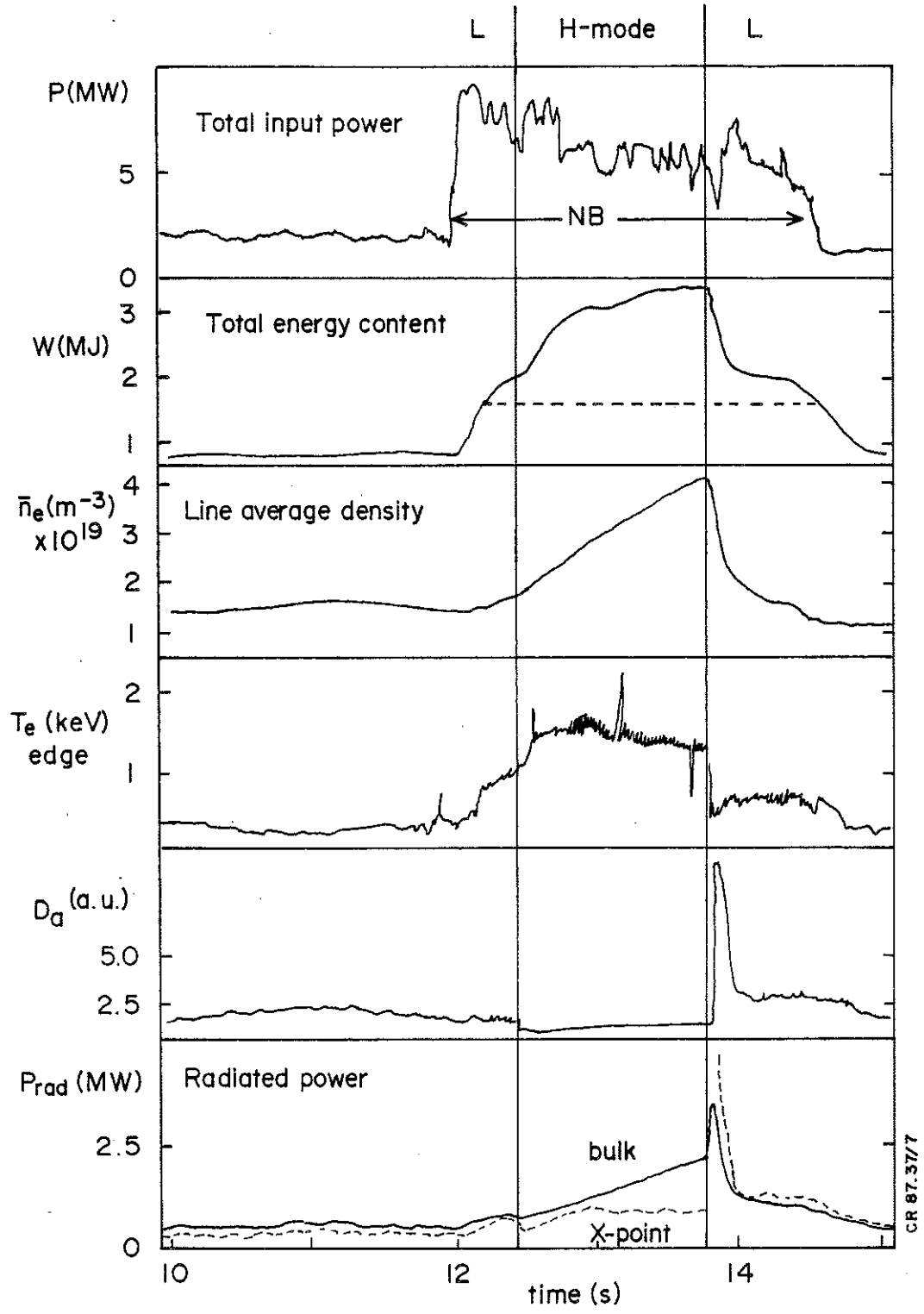

Fig 6 Time evolution of neutral beam heated single null discharge. Plasma current = 2.0MA, toroidal field = 2.2T (Pulse No 10645).

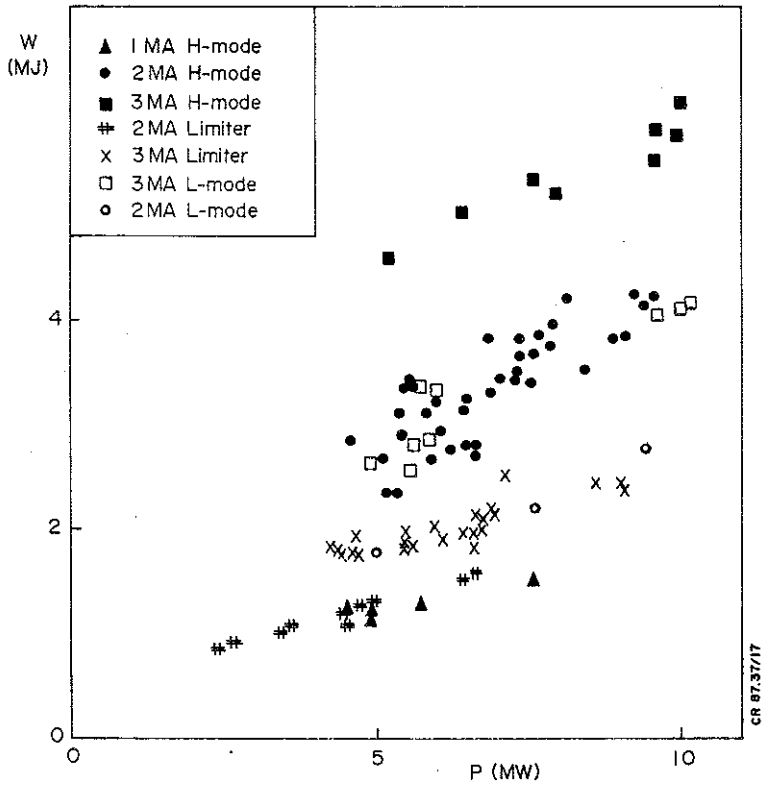

Fig 7 Total stored energy, as measured with diamagnetic loop, versus total input power for limiter and L and H-mode discharges, toroidal field = 2.2T.

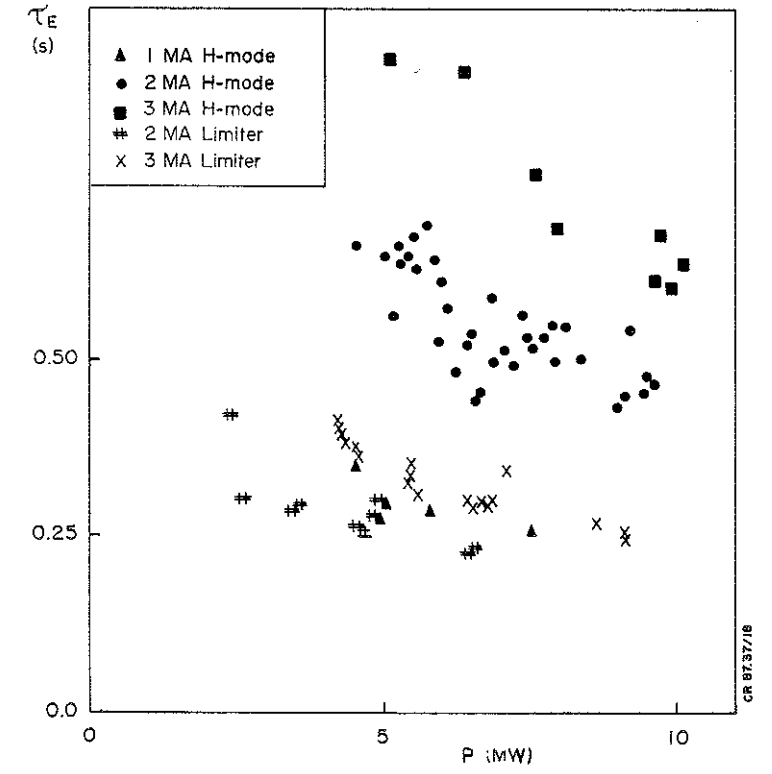

Fig 8 Global energy confinement time measured with diamagnetic loop versus total input power.

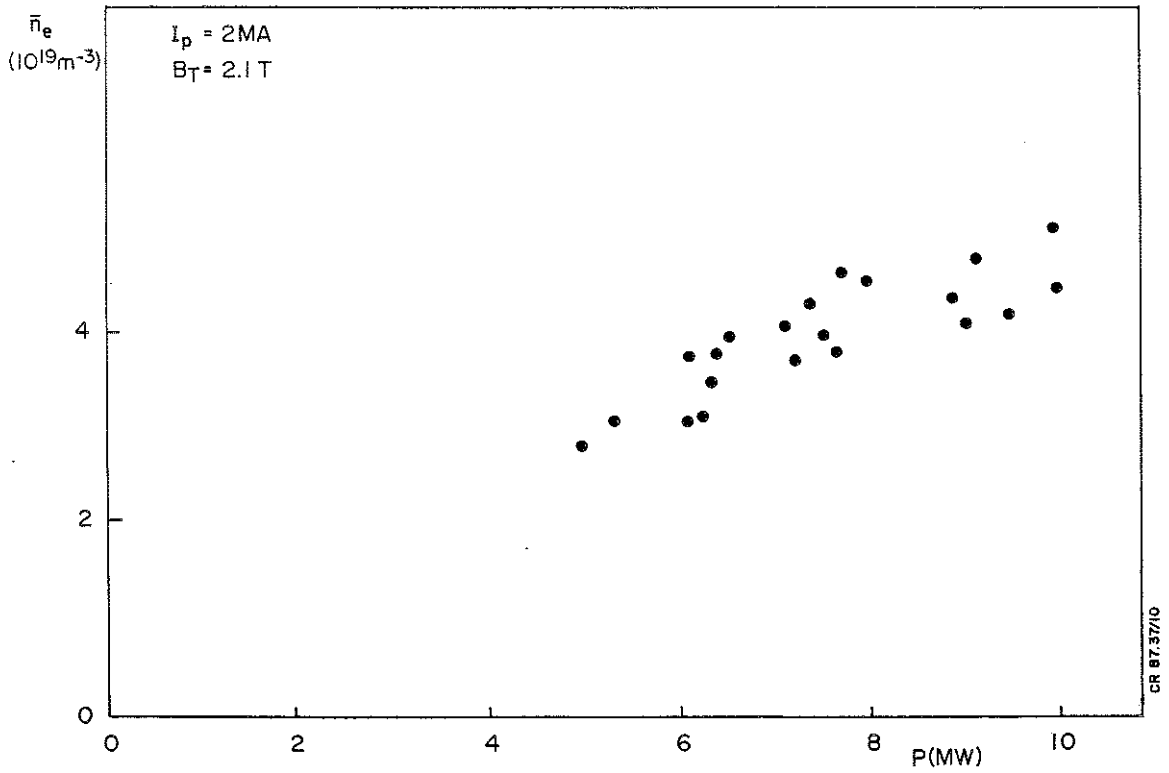

Fig 9 Maximum volume average electron density during the H-mode versus total input power.

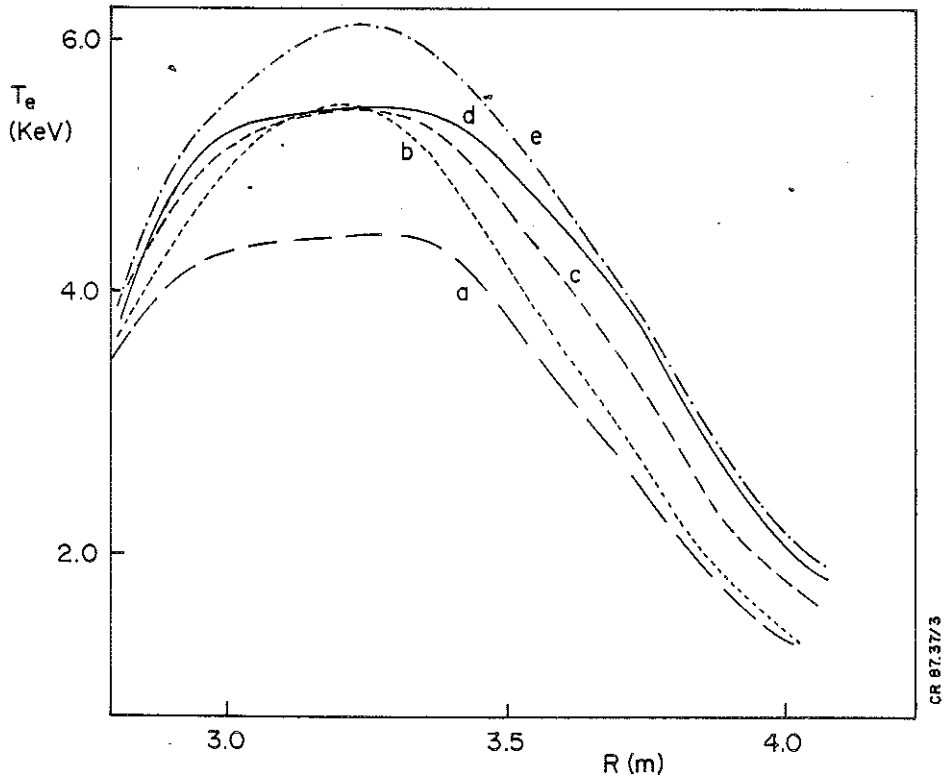

Fig 10 Sequence of ECE profiles showing the L-H transition,(a) is at t = 12.0s,(b) at t = 12.2s,(c) at t = 12.4s; this radial profile coincides with the transition L→H,(d) at t = 13.2s, and (e) at 13.3s. The average plasma density increases during this sequence from 1.7 to $3.5.10^{19}m^{-3}$. (Pulse No 10826, plasma current 2MA, toroidal field 2.8T).

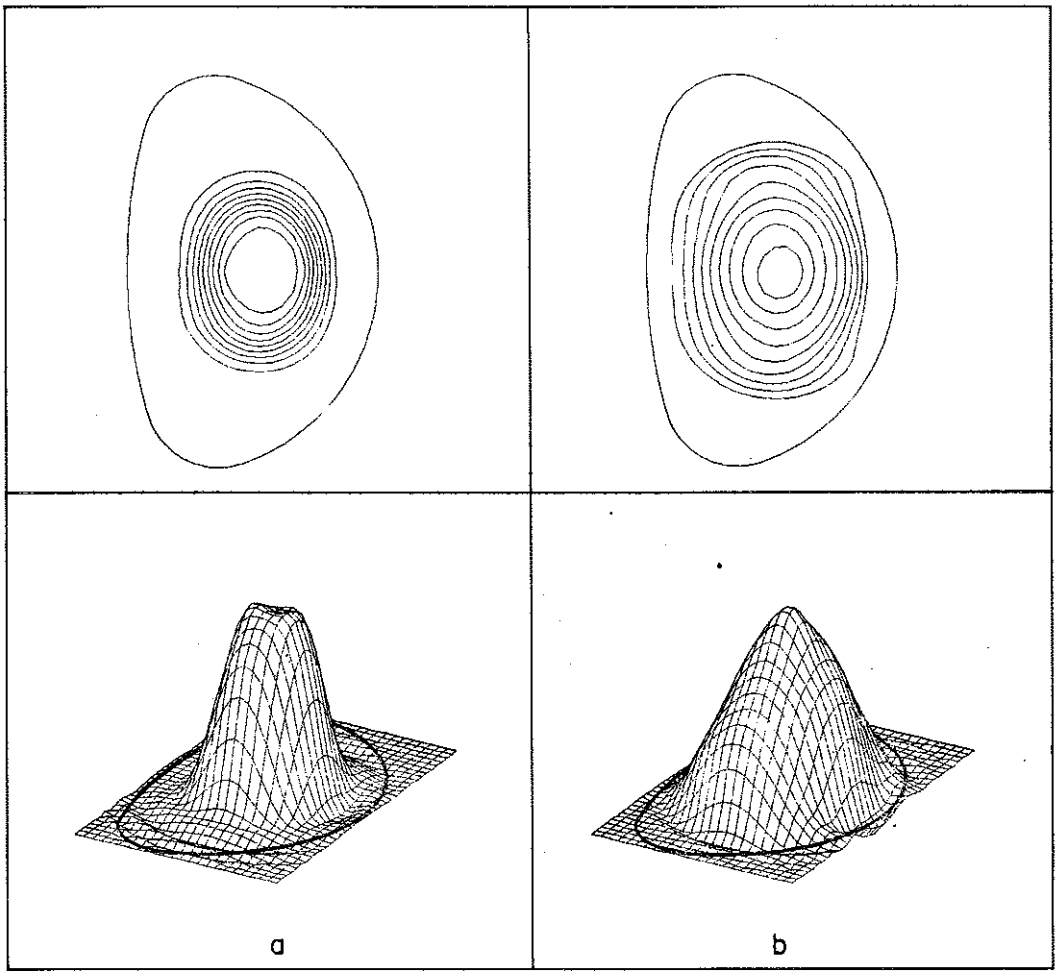

Fig 11 Profiles of soft X-ray emissivity for L and H-mode.

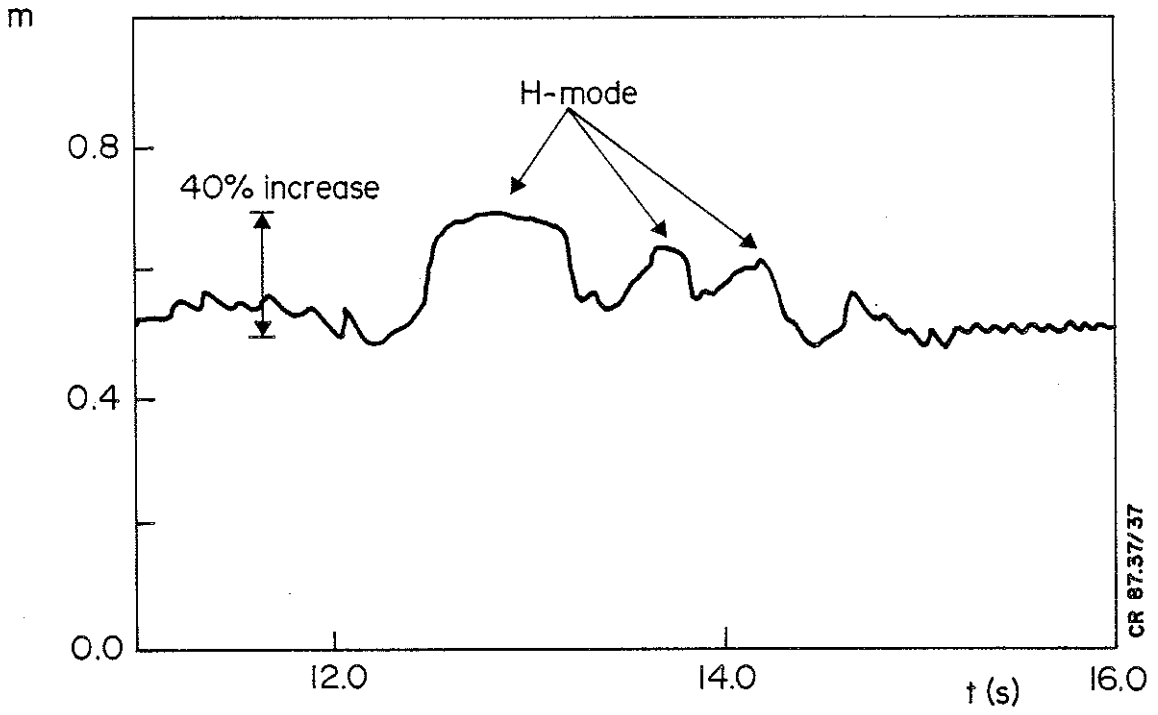

Fig 12 Time evolution of the second moment of the X-ray profile for a discharge with 7MW of total input power.

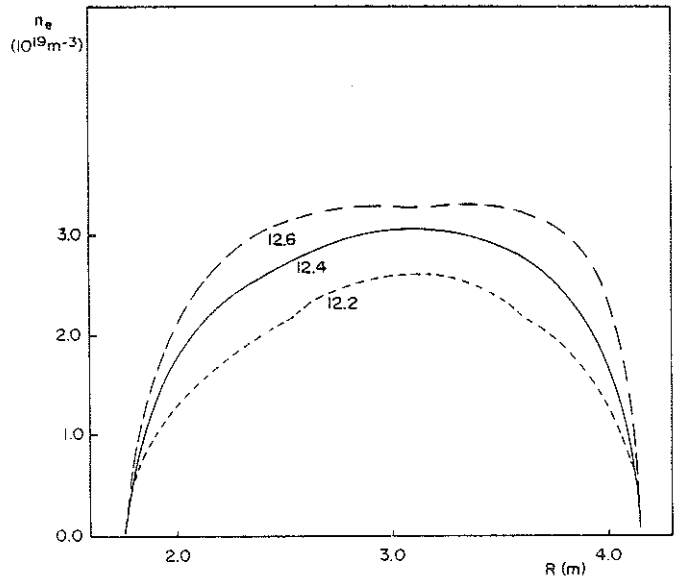

Fig 13 Sequence of electron density profiles from Abel inverted interferometric signals featuring a L-H transition. The profile at t=12.2s is taken in the L-phase, that at 12.6s is in the H-phase.

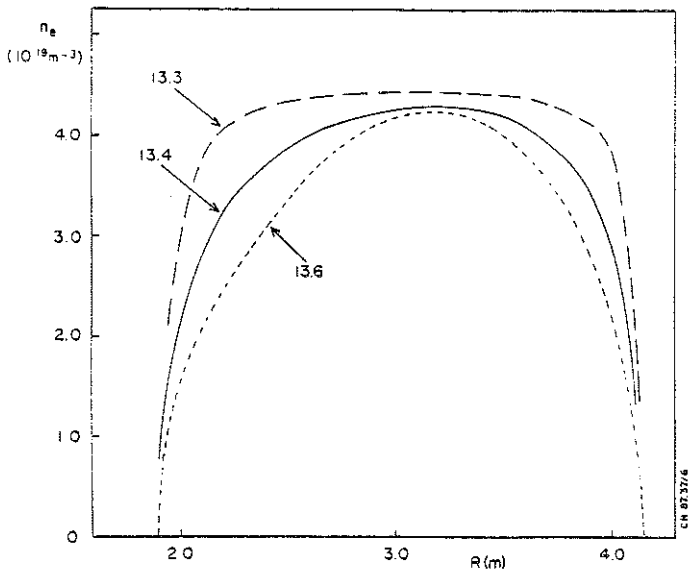

Fig 14 As from Fig 13 but featuring a H-L transition. The profile at t=13.3s is in the H-phase while at t=13.6s the discharge in the L-phase.

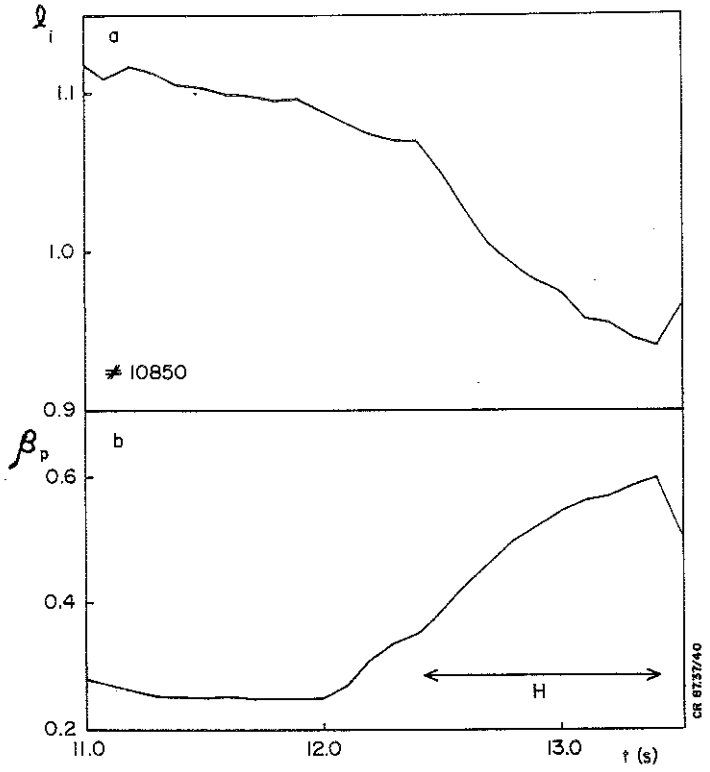

Fig 15 (a) Time evolution of internal inductance during L and H mode.
(b) Time evolution of poloidal beta.

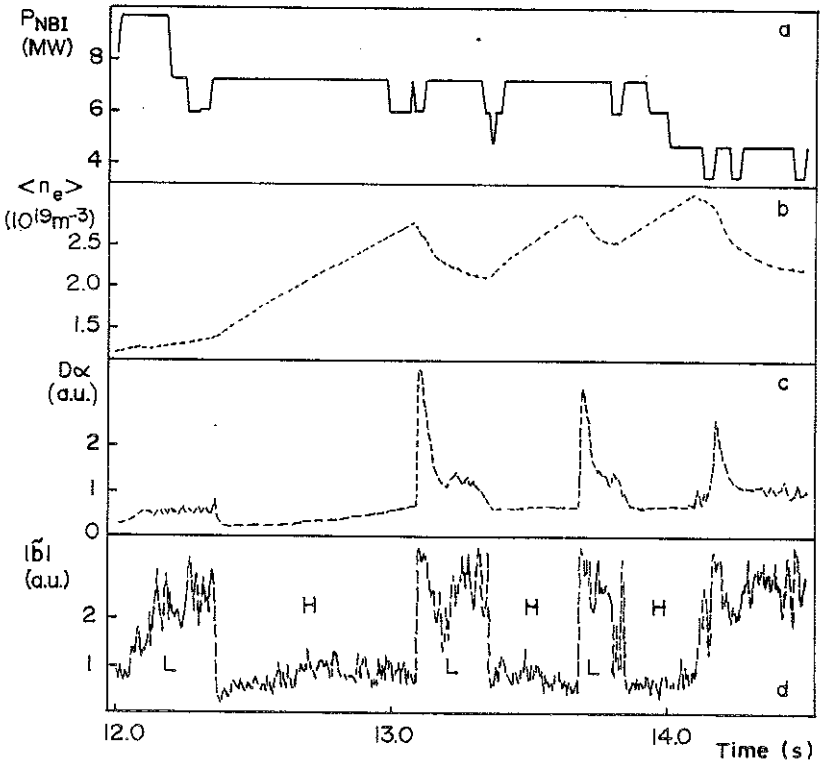

Fig 16 Time evolution of (a) Neutral beam power,(b) average electron density,(c) D_α chord integrated emission,(d) Magnetic fluctuation in a frequency band centred at f = 40kHz. A sequence of three L and H phases is shown.

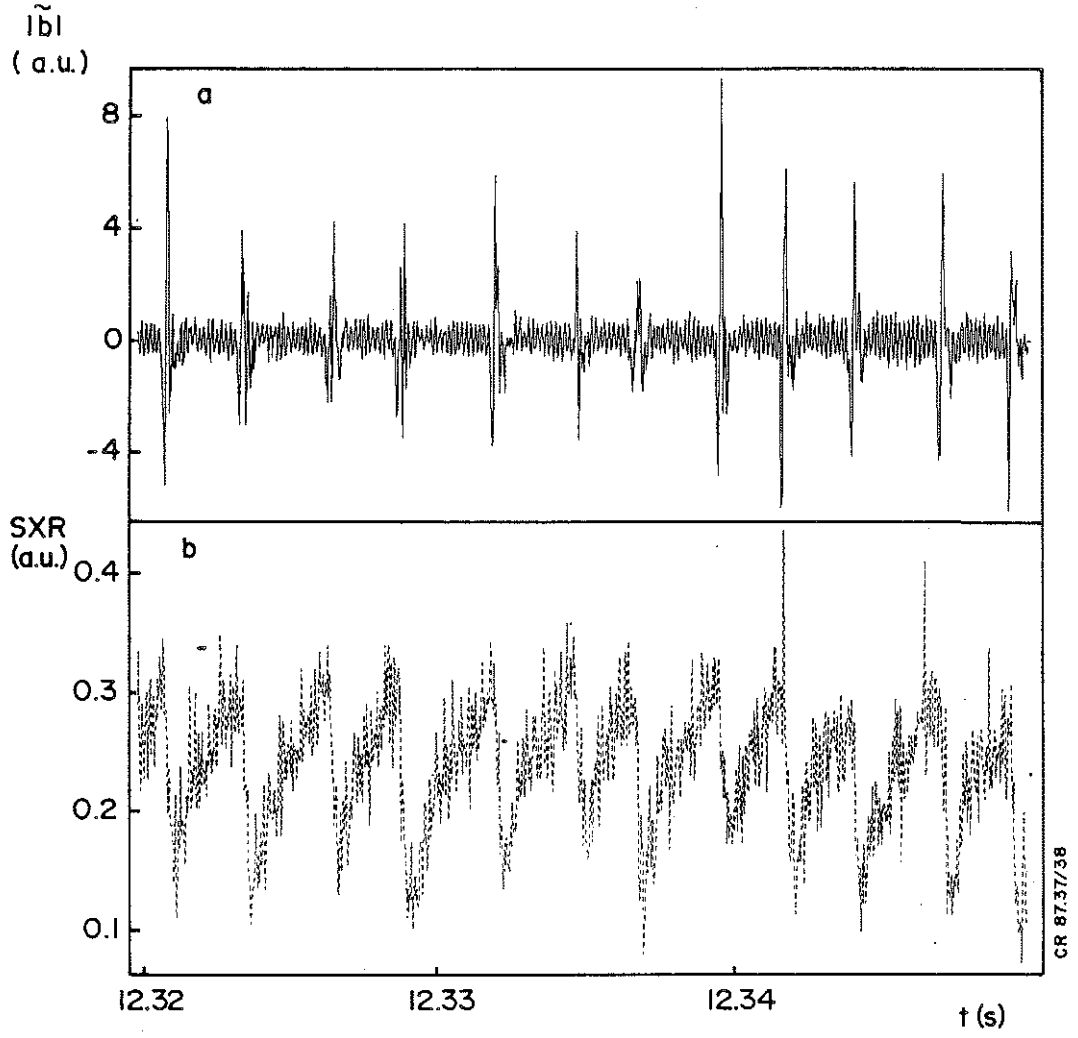

Fig 17 Time correlation between fluctuation from (a) magnetic pick up coil and (b) edge soft X-ray signal.

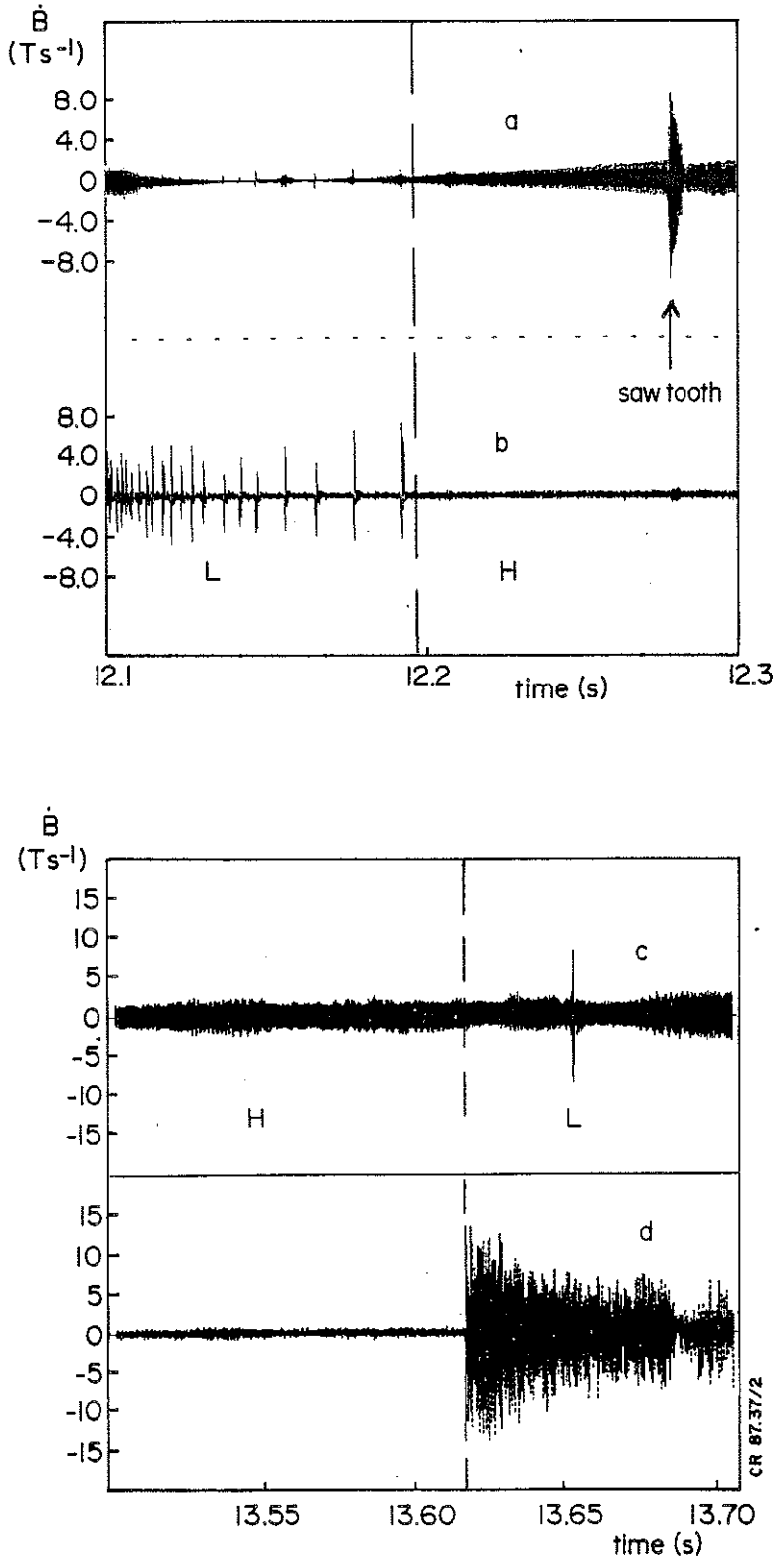

Fig 18 Magnetic fluctuations during the L to H transition;(a) pick up coil near the X-point;(b) pick up coil opposite to the x-point (bottom of the vessel. During H-to L transition: (c) pick up coil near the X-point;and (d) opposite the X-point.

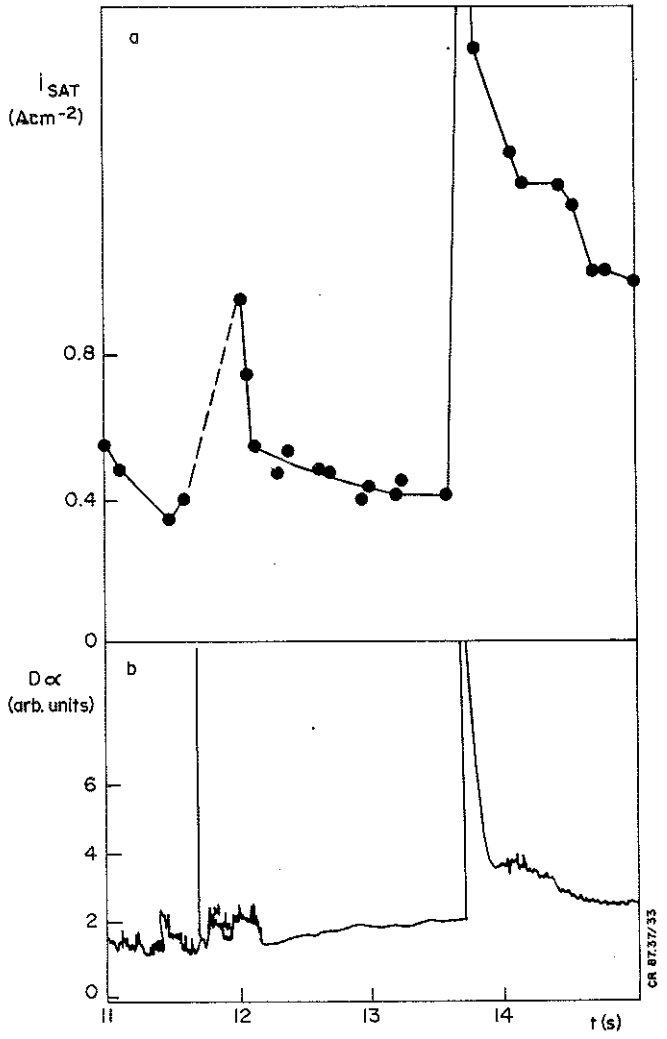

Fig 19 Temporal variation of (a) saturation current measured by a Langmuir probe and (b) D_α signal.

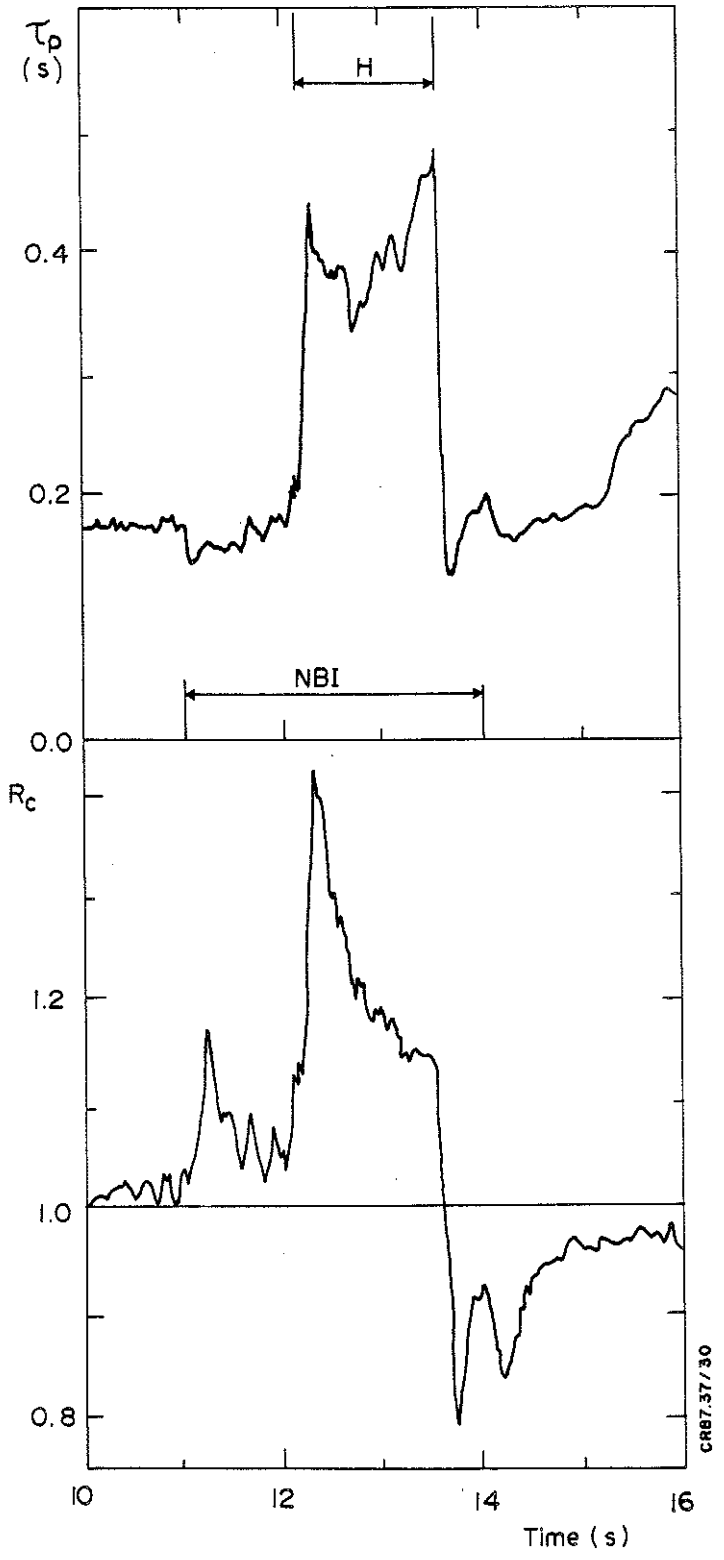

Fig 20 Temporal variation of (a) global particle confinement time during L-H-L mode, (b) Recycling coefficient (Pulse No 10789, plasma current: 3.0MA; total input power - 10MW).

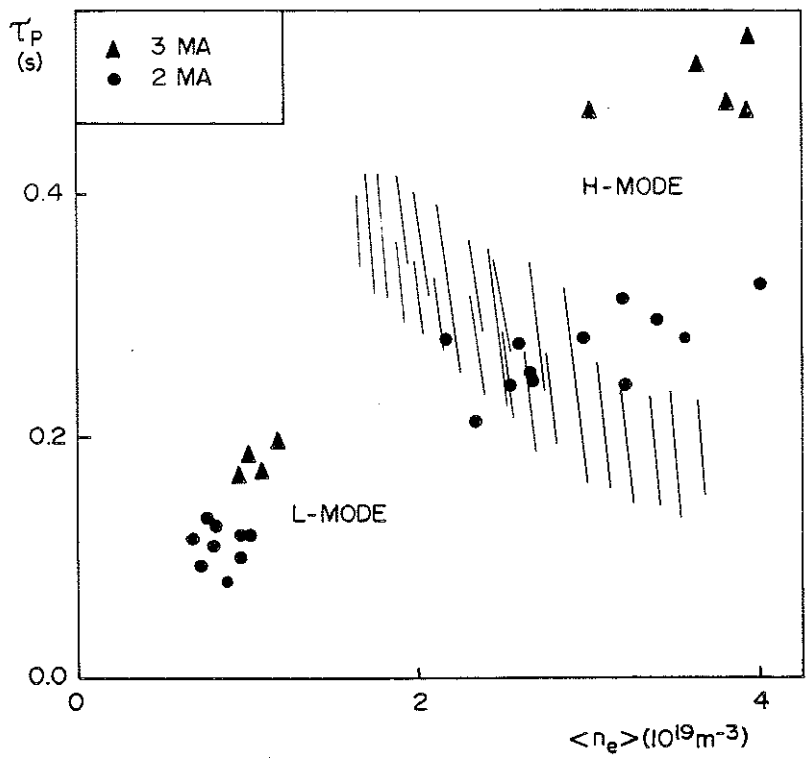

Fig 21 Global particle confinement time versus plasma density for L and H mode discharges. The dashed area is the reference limiter band of values.

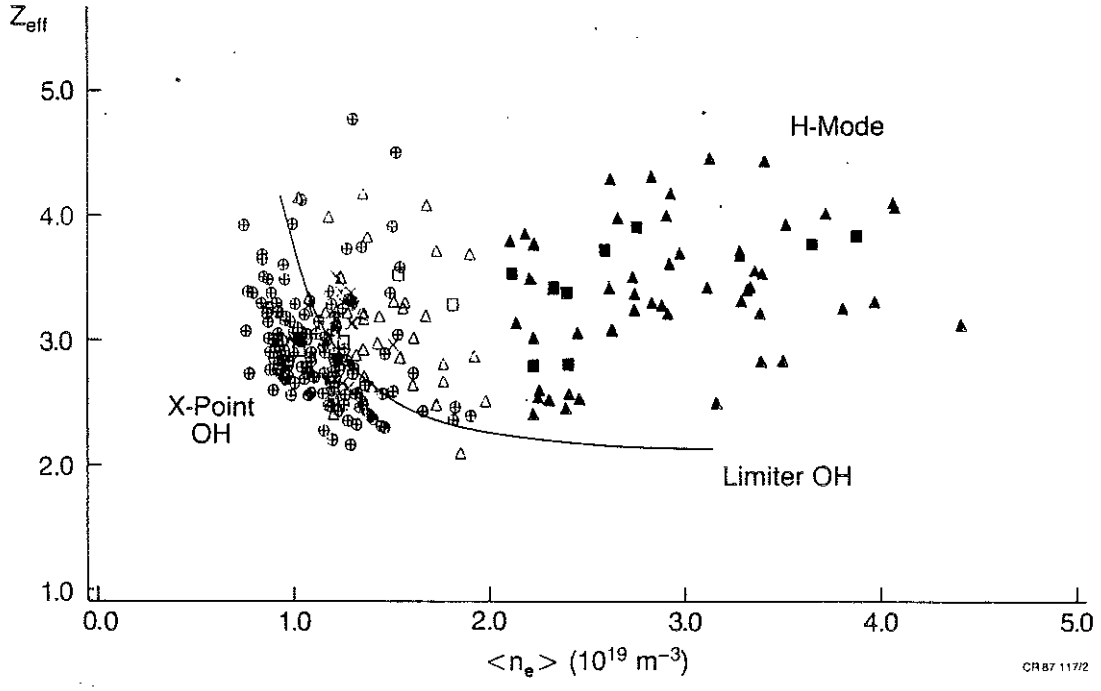

Fig 22 Z_{eff} vs $<n_e>$ for X-point plasmas with ohmic heating (o), NB-heating (Δ) and combined heating ( ) (solid symbols denoting H-mode). For comparison the continuous line shows the typical behaviour of limiter plasmas with ohmic heating is shown. In the H-mode, Z_{eff} does not decrease as normal with higher $\bar{n}_e$.

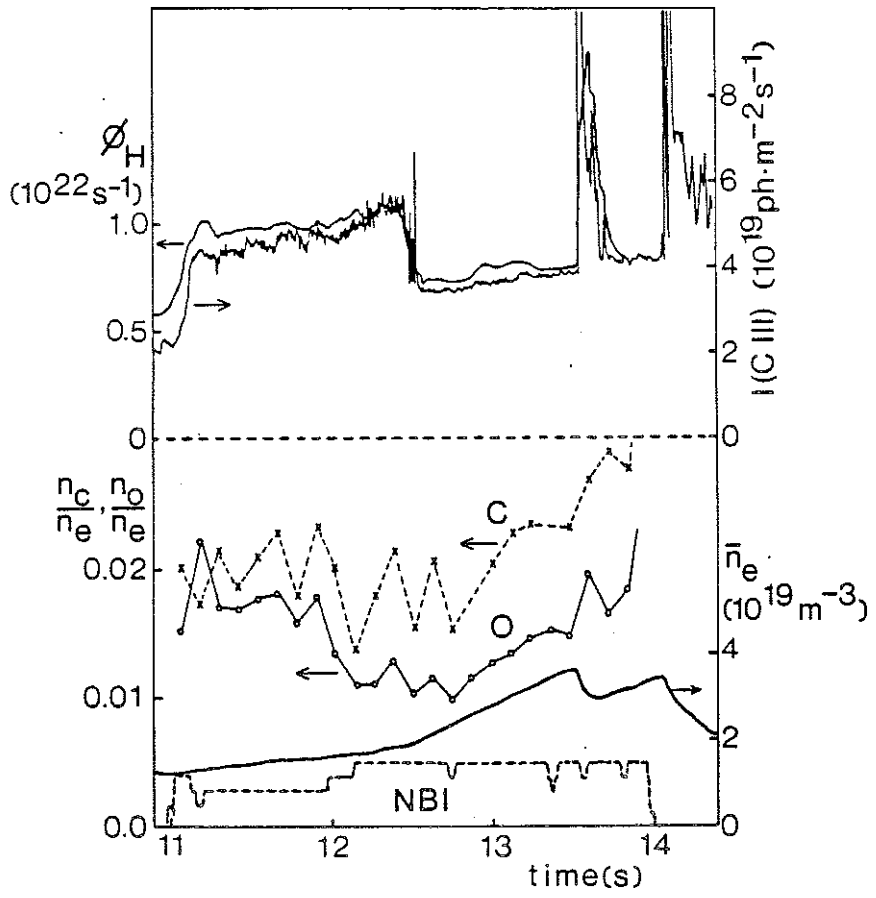

Fig 23 Behaviour of line average electron density ($\bar{n}_e$), carbon and oxygen concentrations (from CXRS), hydrogen flux (ϕ_H), and carbon influx, represented by the brightness of a C III-line (vertical viewing) during L- and H-mode in a NB-heated (5MW) X-point discharge. The L→H transition takes place at ~12.5s. The confinement of carbon is improved in the H-mode.

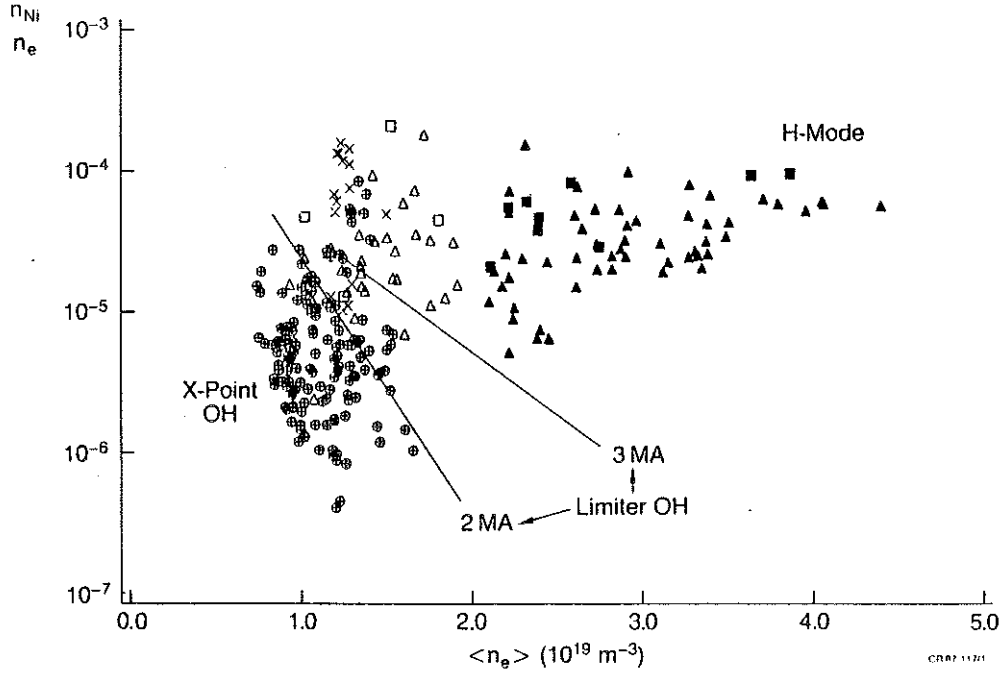

Fig 24 Comparative values of the nickel concentrations vs $\langle n_e \rangle$. Same symbols are the same as in Fig 22. For comparison the lines show the trend for ohmic limiter dishcarges at 2MA and 3MA.

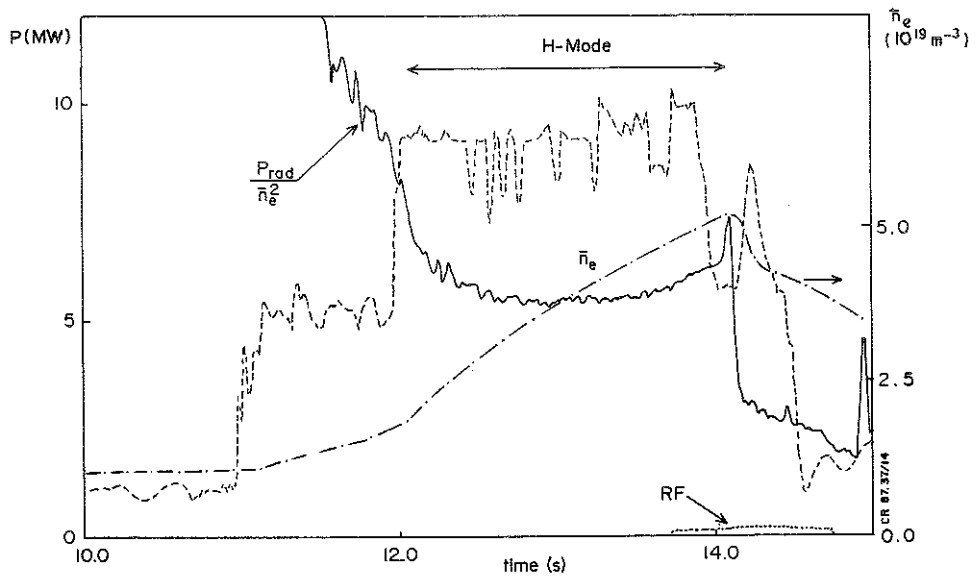

Fig 25 Time variation of the ratio of the radiated power from the main plasma to the square of the average plasma density during L and H-mode (#10755), P is the total input power, $\bar{n}_e$ is the line average density.

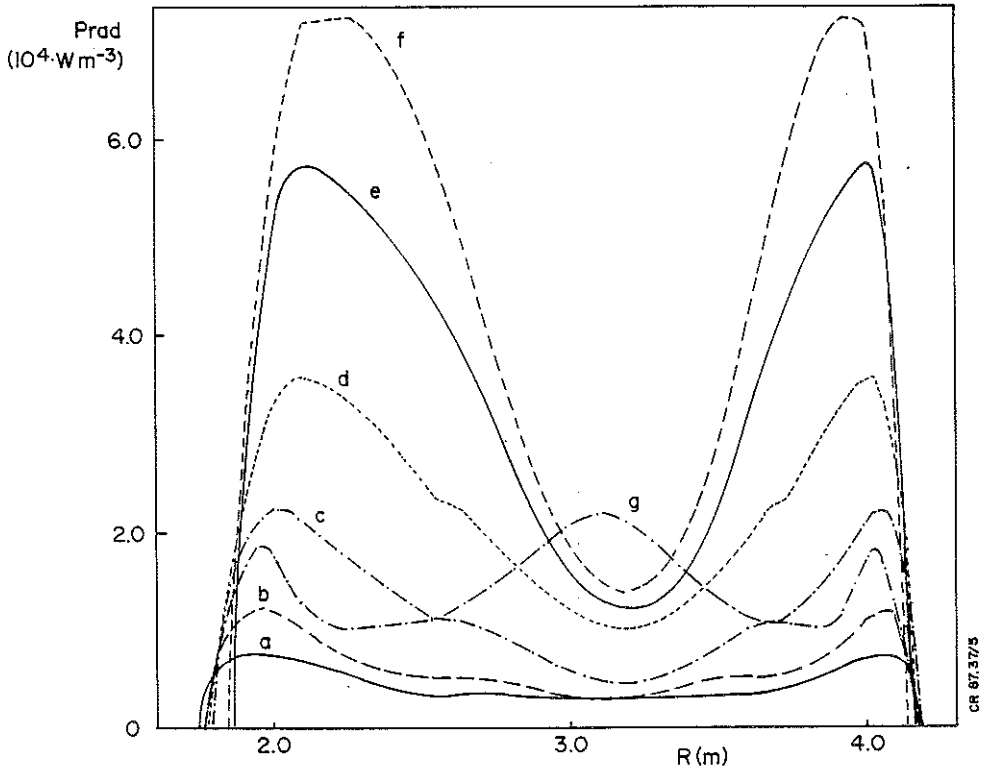

Fig 26 Sequence of Abel inverted radiation profiles for the same pulse of Fig 25. (a) is at 11.3s, (b) at 11.9s, (c) at 12.5s, (d) at 13.1s, (e) at 13.7, (f) at 14.0s at the end of the H phase, and (g) at 14.3 is just after the H→L transition.

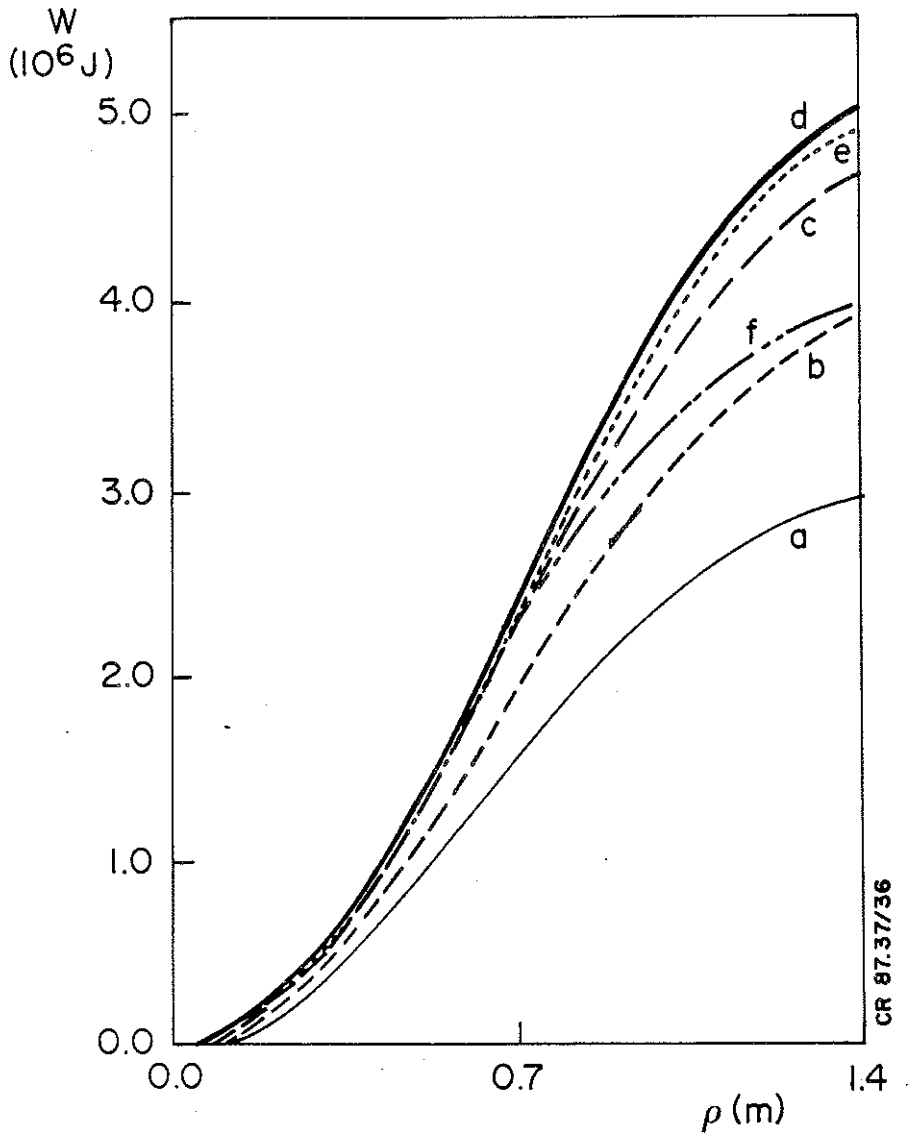

Fig 27 Radial profile of the total plasma stored energy for pulse 10755. Times: (a) t=12.2s; (b) t=12.5s; (c) t=12.8s; (d) t=13.0s; (e) t=13.4s and (f) t=13.7s. The horizontal axis is the average plasma radius over iso - ψ surfaces.

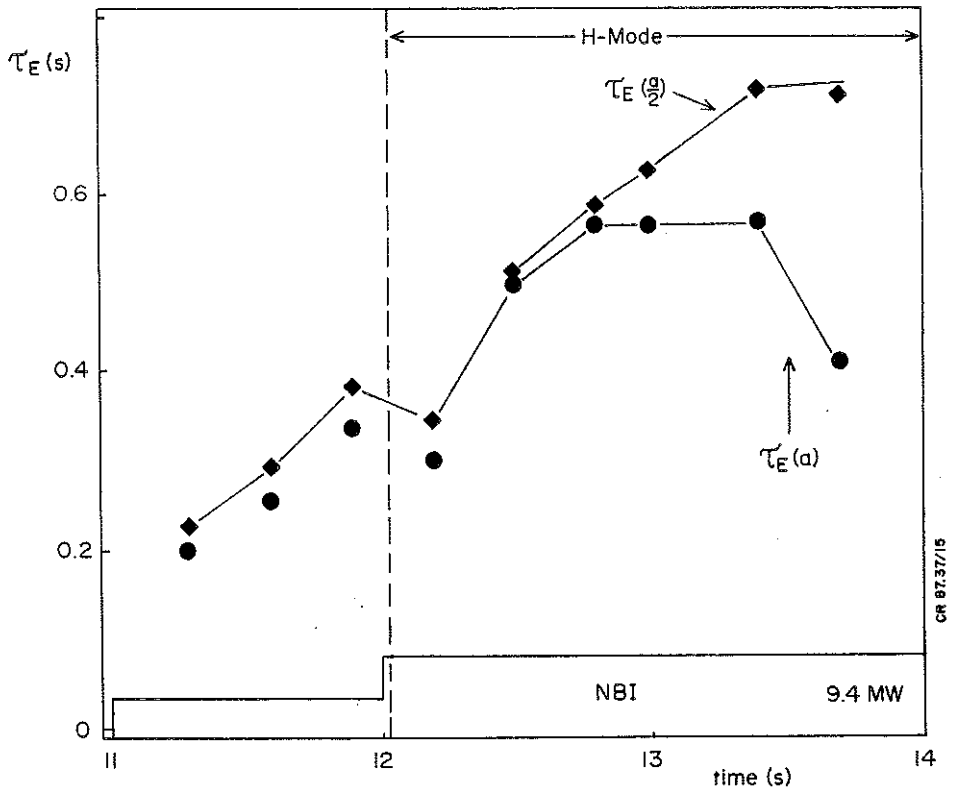

Fig 28 Comparison of time evolution of energy confinement time at half of the plasma radius and the global values, from kinetic data (# 10755).

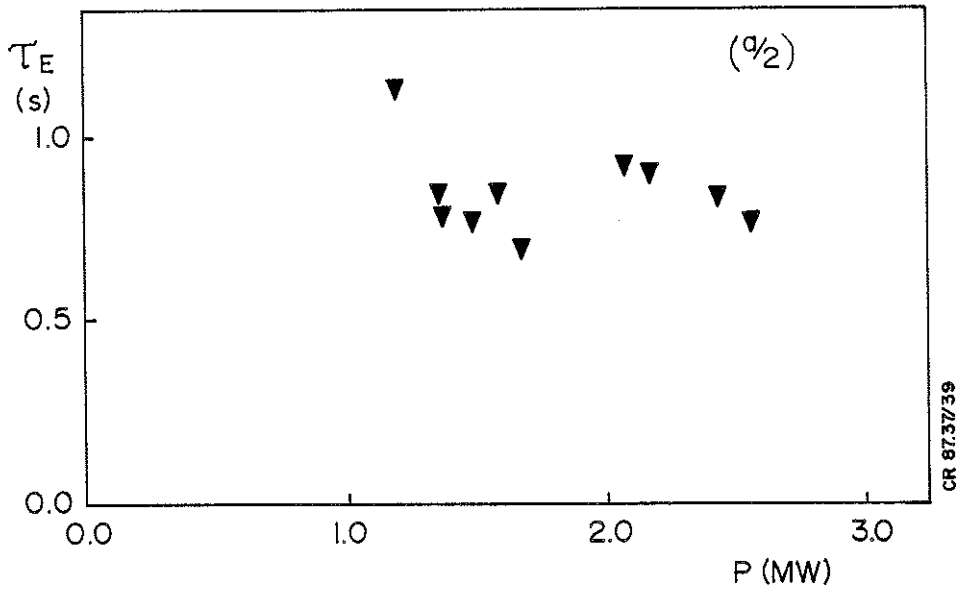

Fig 29 Confinement time at half plasma radius versus total input power calculated from kinetic data of a series of three discharges.